PHYSICAL AND CLINICAL PERFORMANCE CHARACTERIZATION OF FUJI XG-1 COMPUTED RADIOGRAPHY SYSTEM

KUMUTINEE PAIRAT

A THESIS SUBMITTED IN PARTIAL FULFILLMENT
OF THE REQUIREMENTS FOR
THE DEGREE OF MASTER OF SCIENCE
(MEDICAL PHYSICS)
FACULTY OF GRADUATE STUDIES
MAHIDOL UNIVERSITY
2006

ISBN 974-04-7881-6

Thesis
Entitled

PHYSICAL AND CLINICAL PERFORMANCE CHARACTERIZATION OF FUJI XG-1 COMPUTED RADIOGRAPHY SYSTEM

Kumutinee Pairat
.....
Miss. Kumutinee Pairat
Candidate

.....
Asst. Prof. Napapong Pongnapang,
Ph.D. (Medical Physics)
Major-Advisor

.....
Asst. Prof. Bancha Ongvilawan,
M.D.
Co-Advisor

.....
Prof. Dr. M.R. Jisnuson Svasti,
Ph.D.
Dean
Faculty of Graduate Studies

.....
Assoc. Prof. Vipa Boonkitticharoen,
Ph.D. (Radiation Biology)
Chair
Master of Science Programme
in Medical Physics
Faculty of Medicine
Ramathibodi Hospital

Thesis
Entitled

PHYSICAL AND CLINICAL PERFORMANCE CHARACTERIZATION OF FUJI XG-1 COMPUTED RADIOGRAPHY SYSTEM

was submitted to the Faculty of Graduate Studies, Mahidol University
for the degree of Master of Science (Medical Physics)
on
November 1, 2006

Kumutinee Pairat
.....
Miss. Kumutinee Pairat
Candidate

.....
Assoc. Prof. Anchali Krisanachinda
Ph.D. (Medical Radiation Physics)
Chair

.....
Asst. Prof. Bancha Ongvilawan
M.D.
Member

.....
Asst. Prof. Napapong Pongnapang,
Ph.D. (Medical Physics)
Member

.....
Prof. Dr. M.R. Jisnuson Svasti,
Ph.D.
Dean
Faculty of Graduate Studies
Mahidol University

.....
Prof. Rajata Rajatanavin,
M.D., F.A.C.E.
Dean
Faculty of Medicine
Ramathibodi Hospital,
Mahidol University

ACKNOWLEDGEMENTS

I would like to express my great gratitude and deepest appreciation to Asst. Prof. Napapong Pongnapang, Ph.D., my major advisor for his guidance, invaluable advice, supervision, constructive comments, and English language proof in this research. I am equally grateful to Asst. Prof. Bancha Ongvilawan, MD., my co-advisor for his help in the experiment, for his kind help of giving beneficial suggestions in the line with verifying clinical aspect of radiographs.

I would like to deeply thank to my thesis committee, Assoc. Prof. Anchali Krisanachinda, Ph.D. Chief Physicist at Section of Nuclear Medicine, Department of Radiology, Faculty of Medicine, Chulalongkorn University for her kind and also the suggestions for the improvement. She was the external examiner Chair of the thesis defense.

I would like to deeply thank Assoc. Prof. Dr. Vipa Boonkitticharoen, Director of School of Medical Physics for her advice and comments in the research proposal.

I wish to thank Department of Radiological Technology, Faculty of Medical Technology, Mahidol University for the permission to use x-rays and CR facilities. I also wish to thank my close friends, my friends at School of Medical Physics and my colleagues for their helps and encouragement through the entire course of study.

I am grateful to all teachers, lecturers and staffs in School of Medical Physics at Division of Radiation Oncology and Nuclear Medicine, Ramathibodi Hospital for their kind support and supply the knowledge in Medical Physics Program.

Finally, I am grateful to my family for their financial support, entirely care, love and understanding during the entire course of study.

Kumutinee Pairat

PHYSICAL AND CLINICAL PERFORMANCE CHARACTERIZATION OF FUJI XG-1 COMPUTED RADIOGRAPHY SYSTEM

KUMUTINEE PAIRAT 4637067 RAMP/M

M.Sc. (MEDICAL PHYSICS)

THESIS ADVISORS:NAPAPONG PONGNAPANG, PH.D.(MEDICAL PHYSICS), BANCHA ONGVILAWAN ,M.D.

ABSTRACT

The study was carried out to evaluate physical and clinical performance of a Fuji XG-1 computed radiography system in regards to physical and clinical image quality. A total of 85 radiographs obtained from anthropomorphic phantom using ±10 and ±20% variation of radiation exposures by changing mAs from standard radiographic techniques were assessed for clinical quality composite index (CQCI) by a qualified radiologist blinded to the experiment. The measurements of Entrance Skin Air Kerma (ESAK) were also independently performed to assess the absorbed dose values from each radiographic examination.

Spatial resolution in lp/mm of 2.2, 2.2 and 2.5 in both scan directions and 20%MTF in lp/mm of 1.65, 1.69 and 2.25 in scan direction and 1.91, 1.91 and 2.17 in sub-scan direction were observed from the image plate sizes of 35 x 43, 35 x 35 and 18 x 24 cm^2, respectively. Percent contrast between 2.19-3.83% was observed. Increasing radiation exposure improved detectability with detection ratio ranges between 0.82-0.88. The exit exposure to image plate of 2 mR was found to be of optimal value for standard size patients. Results showed that ESAK values obtained from all radiographic examinations ranges between 57-89% lower than IAEA BSS guidance levels. Image quality obtained from 20% variation of mAs, which directly related to ESAK was also found to be insignificantly different. This suggests 20% reduction in radiation dose to patient could possibly be achieved. No significant correlation was found between the patient dose and CQCI except in chest PA and T spine examinations.

KEY WORDS: COMPUTED RADIOGRAPHY (CR) / IMAGE QUALITY / ENTRANCE SKIN AIR KERMA (ESAK) / CLINICAL QUALITY COMPOSITE INDEX (CQCI)

75 P. ISBN 974-04-7881-6

การประเมินคุณสมบัติเชิงฟิสิกส์และคลินิกของเครื่องถ่ายภาพรังสีคอมพิวเตอร์ FUJI XG-1 (PHYSICAL AND CLINICAL PERFORMANCE CHARACTERIZATION OF FUJI XG-1 COMPUTED RADIOGRAPHY SYSTEM)

กุมุทินี ไพรัตน์ 4637067 RAMP/M
วท.ม. (ฟิสิกส์การแพทย์)

คณะกรรมการควบคุมวิทยานิพนธ์ : นภาพงษ์ พงษ์นภางค์, Ph.D. (MEDICAL PHYSICS),
บัญชา องค์วิลาวัณน์, พ.บ.

บทคัดย่อ

การศึกษาในครั้งนี้มีวัตถุประสงค์เพื่อประเมินคุณภาพของภาพถ่ายจากเครื่องถ่ายภาพรังสีคอมพิวเตอร์ FUJI XG-1 โดยศึกษาทั้งทางคุณสมบัติทางฟิสิกส์และทางคลินิค โดยทางคลินิกทำการถ่ายภาพรังสีทั้งสิ้น 85 ภาพ และใช้ค่าปริมาณรังสี ให้อยู่ระหว่าง ±10% และ±20% จากค่ามาตรฐานที่ใช้งานทางคลินิก จากนั้นทำการประเมินผลภาพถ่ายที่ได้ด้วย Clinical Quality Composite Index (CQCI) โดยรังสีแพทย์พร้อมทั้งวัดปริมาณรังสี Entrance Skin Air Kerma (ESAK) ที่ผิวผู้ป่วยในแต่ละภาพ

ผลการศึกษาที่แผ่นรับสัญญาณภาพ 3 ขนาด (ได้แก่ 35 x 43, 35 x 35, 18 x 24 cm^2) พบว่า ค่า Spatial resolution มีค่าเท่ากับ 2.2, 2.2 และ 2.5 lp/mm ทั้งการสแกนทั้งสองแนวสแกน และพบว่าค่า Modulation Transfer Function (MTF) ที่ 20 % มีค่าเท่ากับ 1.65, 1.69 และ 2.25 lp/mm ในทิศทางแนวสแกน และ 1.91, 1.91 และ 2.17 lp/mm ในทิศทางตั้งฉากกับแนวสแกน ตามลำดับ ค่า low contrast detectability ดีขึ้นเมื่อปริมาณรังสีเพิ่มขึ้น โดยมีค่าเปอร์เซ็นต์ความแตกต่างอยู่ในช่วง 2.19-3.83 % และค่าสัดส่วนที่นับวัดได้ (Detection Ratio) อยู่ในช่วง 0.82-0.88 ค่าปริมาณรังสีที่เหมาะสมสำหรับผู้ป่วยขนาดมาตรฐานที่ผ่านมายังแผ่นรับสัญญาณภาพ พบว่า มีค่าเท่ากับ 2 mR และเมื่อทำการวัดค่า ESAK จากทุกภาพ พบว่าค่าที่ได้มีค่าน้อยกว่าค่ามาตรฐานของ IAEA BSS กำหนดไว้อยู่ 57-89% ซึ่งถึงแม้ว่าได้ทำการผันแปรค่า mAs ไปก็ไม่ทำให้เกิดการเปลี่ยนแปลงของค่า CQCI ลงอย่างมีนัยสำคัญ ดังนั้นการลดปริมาณรังสีแก่ผู้ป่วยลง 20 %จึงเป็นไปได้ โดยคุณภาพภาพยังอยู่ในมาตรฐานที่กำหนด ยกเว้นในการถ่ายภาพบริเวณทรวงอก

75 หน้า. ISBN 974-04-7881-6

CONTENTS

LIST OF TABLES

LIST OF FIGURES

LIST OF FIGURES (Continued)

LIST OF FIGURES (Continued)

LIST OF ABBREVIATIONS

Abbreviation	Term
AAPM	American association of physicist in medicine
ACR	American college of radiology
AP, PA	Anteroposteria, Posteroanteria
BSS	Basic safety standard
Cm	Centimeter
CQCI	Clinical quality composite index
CR	Computed radiography
ESAK	Entrance skin air kerma
ESD	Entrance skin distance
FCD	Focal to chamber distance
FED	Focal to entrance distance
FID	Focal to image distance
HVL	Half value layer
IAEA	International Atomic Energy Agency
ICRUM	International Commission on Radiation Unit and Measurements
IP, IPs	Image plate, Image plates
IPEM	Institute of physics and engineering in medicine
kVp	Kilovolt (peak)
Lp/mm	Linepair per millimeter
LSF	Line spread function
mA, mAs	Milliampere, Milliampere-second
mR	MilliRoentgent
MTF	Modulation transfer function
PACS	Picture archiving and communications system
PSL	Photostimulated luminescence
QCP	Quality control program

CHAPTER 1
INTRODUCTION

At the 1981 International Congress of Radiology meeting in Brussels, Fuji Photo Film Co., Ltd., introduced the concept of computed radiography employing photostimulable phosphor plate technology. In 1983, computed radiography was first used clinically in Japan, and was in widely use at the turn of the century as many departments installed Picture Archiving and Communications System (PACS), often in concert with the development of the electronic medical record.[1]

Present day, Computed Radiography (CR) is based on the use of photostimulable phosphors, which are also known as storage phosphors.[2] They are commercially the most successful detectors for digital radiography. The phosphors used are most often in the barium fluorohalide family in power form and deposited onto a substrated to form an image plate or screen.[3] X-ray absorption mechanisms are identical to those of conventional phosphor screens used with film. They differ in that the useful optical signal is not derived from the light emitted in prompt response to the incident radiation, but rather from subsequent emission when the latent image, consisting of trapped charge , is optically stimulated and released from metastable traps. This triggers a process called photostimulated luminescence (PSL) resulting in the emission of shorter wavelength (blue) light in an amount proportional to the original x-ray irradiation. In CR, an image plate (IP) containing the storage phosphor is positioned in a light-tight enclosure, exposed to the x-ray image and then read out by faster scanning with a laser to release the PSL. The blue PSL light is collected with a light guide and detected with a photomultiplier tube (PMT). The PMT signal is digitized to form the image on a point-by-point basis.[4] The digital image that is generated by the CR reader is stored temporary on a local hard disk. Many CR systems are joined (“docked”) directly to laser printers that make film hard copies of the digital images. CR systems often serve as entry points into a PACS, and in such

cases the digital radiographic image is sent to the PACS system for interpretation by the radiologist and long-term archiving.[5]

PACS is a sister technology of teleradiology that also allows storage and archiving, as well as transmission, of digital images within an enterprise-typically a hospital. A teleradiology system consists of an image acquisition section and image display/interpretation, connected by a communications system (i.e., a network). The most important aspects of a teleradiology system are its costs and clinical effectiveness. Key points are the reliability of the system, the quality of the displayed images, the speed of access to the images, and the ease of use. The system should have adequate storage capacity to retain images for at a least one week, unless hard copy is going to be stored. In many countries is a legal requirement to store images for periode of years. Also, it should be possible to select and display previous images together with current images, with enlargement of selected areas. The accessibility of images on a computer network, which is an important aspect of teleradiology and critical to PACS will bring about significant changes in the practice of radiology in the future. It will be possible for clinicians to view digital radiographs on a display outside radiology departments, with rapid access to current and previous images. Also, look for computer-aided diagnosis in the future. In many countries, economic developments are more rapid than the development of their health care infrastructures, and demands for high quality radiology may be met more easily using teleradiology.[6]

In digital radiography the exiting radiation intensity is converted into an electronic form that is digitized and numerically encoded into discrete picture elements (or “pixels”). The spatial resolution of the digital matrix is determined by the number of pixels per unit area. The radiation energy absorbed in the detector may be temporarily captured in a medium that produces light in proportion to the amount of radiation absorbed. The light is converted into an electronic signal that can be amplified before transmission to an analog-digital converter that divides the signal strengths into discrete steps. The contrast resolution, or fineness with which each pixel can resolve differences in radiation intensity (i.e., “gray-scale resolution”). The additional digital gray scale can actually be utilized (and perceived) by the trick of electronically adjusting the window level and width of the image data presentation

(i.e., equivalent to changing the environment of the eve to a new specific adaptation condition).[7-9] In digital imaging high gray-scale resolution is very desirable because it permits the detection of very slight differences in radiation attenuation that may not be appreciated with film. This is especially true for digital radiographs obtained with storage phosphor detectors that have a wide dynamic range in the initial data acquisition of the latent image.

It seems reasonable to design digital systems with individual components that produce the highest possible levels of spatial and contrast resolution, but this is neither feasible nor truly desirable. A carefully considered compromise in spatial and contrast resolution must be reached in order to avoid unnecessarily complex image processing, prolong processing time, wasteful display requirements, long transfer times, unnecessarily high data-storage requirements, and inordinate cost.[10-11] Thus, the spatial and contrast resolution specifications must meet the minimum requirements for clinical practice, but not greatly exceed them. The technical capabilities of the components must be matched to realize their individual potentials. For instance, superior spatial (or contrast) resolution of a detector does little good if either the display or the archival medium has substantially poorer capabilities. The extent to which superiority in one characteristic can compensate for a weakness in another is an important consideration in system design. For example, the relatively lower spatial resolution of many digital systems (as compared to film radiography) may be partially offset in certain clinical tasks by the availability of better contrast resolution or scatter rejection.

Overall system performance cannot be judged by technical characteristics alone. In the final analysis, the value of digital radiography must be judged by its comparative diagnostic performance against conventional film radiography, irrespective of the individual technical specifications. It is quite likely that technical differences between modalities may result in superior performance in one task, but inferior performance in another. In many clinical tests of diagnostic performance, state-of-the-art commercial digital radiographic systems meet or exceed the performance of film radiography. In other tasks, however, especially those that rely on high spatial resolution, digital imaging may only be an adequate replacement for film when special image processing routines are employed.

Any medical image can be described in terms of three basic concepts : spatial resolution or clarity, contrast, and noise. Image contrast refers to the difference in the image gray scale between closely adjacent regions on the image.[5] Spatial resolution or clarity refers to the geometrical size of small objects are visible in the image. Noise refers to the precision with which the signal is generated ; a noisy image will have large fluctuations in the signal across a uniform object while a precise signal will have very small fluctuations.[12]

1.1 Spatial resolution[5]

Spatial resolution is a property that describes the ability of an imaging system to accurately depict objects in the two spatial dimensions of the image. Spatial resolution is sometimes referred to simply as the resolution. The classic notion of spatial resolution is the ability of an image system to distinctly depict two objects as they become smaller and closer together. The closer together they are, with the image still showing them as separate objects, the better the spatial resolution. At some point, the two objects become so close that they appear as one, and at this point spatial resolution is lost.

1.2 Physical determinants of contrast[12]

Contrast conceptually refers to the difference in brightness or darkness in the image between an area of interest and its surrounding background. The information in a medical image usually is presented in “shades of gray”. One uses the differences in gray shades to distinguish different tissue types, analyze anatomical relationship, and sometimes quantify physiological function. The larger the difference in gray shades between two different tissue types, the easier it is to make these important clinical distinction. It usually is the objective of a system to maximize the contrast in the image for any particular object of interest.

1.3 Noise[13]

Noise is often defined as the uncertainty in a signal due to random fluctuations in that signal. There are many causes for these fluctuations. For example, an x-ray beam emerging from an x-ray tube inherently is statistical in nature. That is, the number of

photons emitted from the source per unit time varies according to a Poisson distribution. Other sources of random fluctuation are introduced by the process of attenuation in the materials present in the path of the radiation beam (patient, x-ray beam filtration, patient table, detector enclosure) which also is a Poisson process. When electronic detectors are used, the attenuation of radiation by the detector is a random process. In addition, some detectors generate currents from thermal sources which introduce random fluctuations into the signal. The noise source therefore is inherent in the radiographic imaging process, and can be increased by a number of different processes.

1.4 Modulation Transfer Function (MTF)[5]

The Modulation Transfer Function (MTF) of an image system, is a very complete description of the resolution properties of an imaging system. The MTF illustrates the fraction (or percentage) of an object's contrast that is recorded by the imaging system, as a function of the size (i.e., spatial frequency) of the object. The MTF is a plot that demonstrates the resolution capabilities of an imaging system (signal modulation) as a function of spatial frequency. Since low spatial frequencies correspond to large objects, and high spatial frequencies correspond to smaller objects, the MTF is just a description of how an imaging system responds depending on the size of the stimulus. Whereas the MTF is best conceptualized using sine wave, in practice it is measured line spread function (LSF) by stimulating the imaging system to a line. A very narrow lead slit is used to collimate the X-ray beam down to a very thin line. Once the LSF is measured, the MTF can be computed directly from it using the fourier transform (FT), MTF(f) = [FT(LSF(x))]

The largest reduction in radiation exposure is to prevent the ordering of an unproductive x-ray examination, patient exposure can also be reduced by the diagnostician by careful consideration of the numbers and types of radiographs to be taken during the examination. These considerations can also be classified as prescription decisions. In conducting x-ray examinations therefore, the diagnostician should be capable of making the best diagnosis possible and be aware of the quantity and potential risk of the radiation is administering .

Each x-ray examination should be as objective-related as possible to accomplish the diagnosis with the minimum amount of exposure. Most x-ray facilities establish a set of standard examination procedure which specify the number and types of radiographic views to be taken when the procedure is performed. A periodic review of all standard examination procedures should be performed to determine if the established routine is achieving the objectives and whether modifications are warranted.

Important considerations in providing optimal diagnostic information at minimum patient exposure, are the role of radiologic diagnosticians and the information provided. Requests for x-ray examinations should be considered as medical consultations between the clinician and the diagnostician and should stage the diagnostic objective of the examination and detail relevant medical history including results of previous diagnostic x-ray examinations and other relevant tests.[14]

CHAPTER 2
OBJECTIVE

The main objectives of this study are :

1. To study the physical performance of a Fuji XG1 computed radiography system for the following characterizations of
   a. High contrast resolution
   b. Low contrast detectability
   c. Modulation Transfer function (MTF)
2. To assess the limitation of the system clinical use.

The sub-objectives of this study are :

1. To study the Entrance Skin Air Kirma (ESAK) incurred at the technique settings (kVp, mAs), considering the clinical imaging quality of radiographs.
2. To determine the optimal exposure techniques for a Fuji XG1 computed radiography with the optimal image quality and the patient radiation dose.

CHAPTER 3
LITERATURE REVIEW

3.1 Physical performance characterization

Several investigators have studied about physical performance characterization of computed radiography systems. Measurements were made in terms of low contrast detectability, high contrast resolution, noise and Modulation Transfer Function (MTF). These parameters represent the technical quality aspects for the performance of CR devices.

Ehsan Samei et al [15] recommended methods to test the performance of computed radiographic systems, recently reported in the American Association of Physicist in Medicine, AAPM Task Group No.10. including the tests for spatial resolution and low contrast resolution. The recommendations can be used for the acceptance testing of new CR devices as well as routine performance evaluation checks of devices in clinical use. The purpose of the short communication is to provide a summary of the tests recommended by the AAPM task group No.10, to delineate the technical aspects of the tests, to suggest quantitative measures of the performance results, and to recommend uniform quantitive criteria for the satisfactory performance of CR devices. The applicability of the acceptance criteria are verified by tests performed on CR systems in clinical use.

Anthony J et al [16] presented a contrast resolution test object that minimizes the limitations of two contrast resolution test tool (the Leeds Test Object TO.N3, and the RMI low contrast resolution test tool model 151). The test object (UAB contrast resolution test tools) was designed to address the problems of two contrast resolution test tool and consists of copper attenuator plates and 6.1-mm-thick aluminum target plates with each plate having a gradation of 1.1-cm-diam circular attenuation differences or holes. The contrast of the test objects'targets was determined for x-ray tube voltages from 50-130 kVp in 10 kV increments with Cu attenuator thickness of 1, 2, and 3mm of Cu. The methodology employed to calculate the test object target

contrast versus tube potential calibration tables and the experimental validation of this methodology were discussed.

Z.F.Lu et al [17] studied the contrast-detail detectability by using a special contrast-detail phantom with drilled holes of varying diameters (detail) and varying depths (contrast). Images of the phantom were acquired using a range of 60-120 kVp and additional 2 mm aluminum added filtration to the x-ray beam. Evaluation of the image quality was carried out by scoring the threshold target depth along the row of the same target diameter. Detection ratio was calculated by counting the number of detectable targets divided by the total number of targets in the phantom. The overall score was related to the patient entrance skin dose, kVp and the thickness of the scattering material. The patient entrance skin dose was reduced as the additional aluminum filter was added to the x-ray beam. Their finding suggested using a higher kVp setting and additional added filtration would reduce the patient entrance skin dose without compromising the contrast-detail detectability, which was compensated by the contrast manipulation on soft-copy display workstations.

A. Koening, A. Gliere [18] described method used in order to stimulate blurring due to the x-ray source or to the detector is presented. They validate object is an x-ray resolution test pattern usually used to determine spatial frequency characteristics of x-ray system. They used software package, sindbad which dedicated to the simulation of the radiographic process. The result of the simulation, the first image is the acquired radiograph. The second image is the result of a simulation without oversampling; the third image is the result of a simulation carried out using oversampling. The last image, to be compared with the acquired radiograph, has been simulated using oversampling and system MTF. In order to check the system MTF model, a radiograph of 50 microns wide slit used to measure the MTF has been simulated and the system MTF has been re-calculate from synthetic radiograph.

3.2 Clinical performance characterization

In a newly installed system, after completion of the physical acceptance testing and prior to a full clinical utilization, the system characterization should also be evaluated for its clinical performance.

Ehsan Samei et al [15] suggested that the clinical evaluation for various anatomical sizes and views should be tested and customized by the application specialist of the manufacturer with assistance of the diagnostic medical physicist and under the direction of the radiologist who is ultimately responsible for the clinical acceptability of the image. Using radiographic techniques provided by the manufacturer, images of various anthropomorphic phantoms should be acquired with various combinations of collimation and positioning, utilizing the appropriate prescribed anatomical menus of the system. The materials can be used as a handbook for acceptance testing and quality control inspection of CR systems to assure the consistency and reliability of their clinical operation.

The work plan of this study was evaluated the physical and clinical performance of a Fuji XG-1 computed radiography systems in regards of high contrast resolution with scan and sub-scan direction for three imaging plate sizes, Low contrast detectability using two phantom (UAB phantom and contrast-detail phantom) with the same measurement techniques, Modulation Transfer Function (MTF) were analyzed from the line-pair test phantom image with imageJ program. Clinical performance characterization was carried out using radiographic techniques provided by the manufacture with variation of mAs setting between ±10 % and ±20%. The Entrance Skin Air Kerma (ESAK) was also evaluated for common radiographic techniques using Fuji-XG-1 CR system.

CHAPTER 4
MATERIALS AND METHODS

4.1 Materials

4.1.1 Test objects (a human-mimicking phantom)

A patient equivalent anthropomorphic phantom (Anderson/RSD phantom by Bicron®) for X-ray spectra typically used for educational purposes was the main test object in the study. This RSD phantom consists of the anatomic and radio-fidelity of PIXY that formed human-mimicking phantom of an average male with 175 cm in tall and 74 kg in weight. According to the manufacturer, the RSD skeleton met radiation interaction properties of both cortical bone and spongiest as standardized by the International Commission on Radiation Unit and Measurements (ICRUM). A-19 different parts of the phantom were selected representing kinds of anatomical organs of interest in common radiography examinations.[20]

- SHT-1169 (the head with cervical spine)
- LC-1018 (the chest-lung, heart and thoracic spine)
- SPT-1088 (the pelvis including lumbar spine)
- SHT-1149 (the right hand/wrist, natural position)
- SHT-1091 (the left-hand/wrist, oblique position)
- SKT-1113 (the knee joint, natural position)
- SKT-1112 (the knee joint, lateral position)
- SLT-1020 (the lower leg)
- SFT-1096 (the right-foot/ankle, natural position)
- SFT-1100 (the right-foot/ankle, oblique position)

4.1.2 Quality control equipments:

- Gammex/RMI full function meter M242
- Gammex/RMI Collimator and beam test tools M162A

- Gammex/RMI Focal spot test tool M112B
- Gammex/RMI Al HVL attenuator set M115A

4.1.3 Equipments for Acceptance Testing of CR system

- General purpose radiographic X-ray system, Quantum medical imaging Quest HF series, USA (Figure 1)
- Fuji XG1 Computed Radiography system (Figure 2)
- Image plates (IPs) and IP cassettes, 35x43 cm^2, 35 x 35 cm^2 and 18x24 cm^2 (Figure 3)
- An ion-chamber volume 6 cm^3
- Electrometer model 9010 Radical Corporation
- A stand for the ion chamber
- Line-pair test phantom
- UAB phantom
- 1-mm copper plate
- A metric steel ruler (for laser-beam function test)
- Wire mesh test tool
- A stopwatch
- A lead sheet or lead apron (to reduce backscatter)

4.1.4 Equipments for physical and clinical performance characterization

- General purpose radiographic X-ray system, Quantum medical imaging Quest HF series, USA at Faculty of Medical Technology
- Fuji XG1 Computed Radiography system, at Faculty of Medical Technology
- Image plates (Ips) and IP cassettes
- An ion-chamber volume 6 cm^3
- Electrometer model 9010 Radical Corporation
- UAB phantom (Figure 4)
- Contrast detail phantom (Figure 5)
- Copper sheet (1.0 mmCu)(Figure.6)
- Line-pair test phantom (Figure 7)
- Anthropomorphic phantom (Figure 8)

Figure 1 General purpose radiographic X-ray system, Quantum medical Imaging Quest HF series

Figure 2 Fuji XG-1 Computed Radiography system

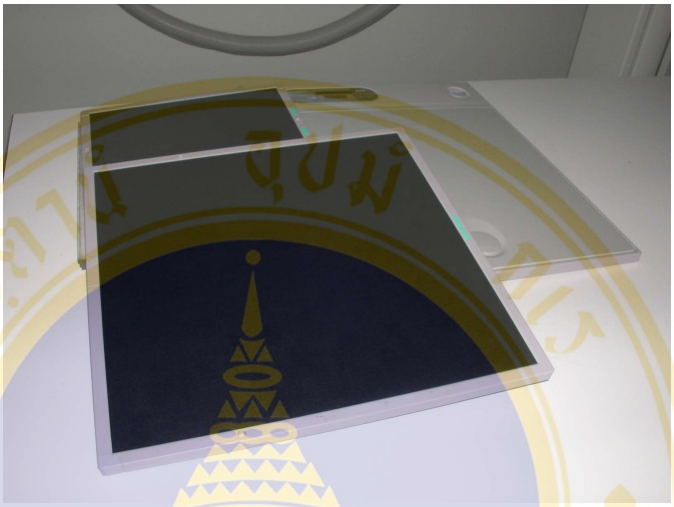

Figure 3 Image plate and image cassettes

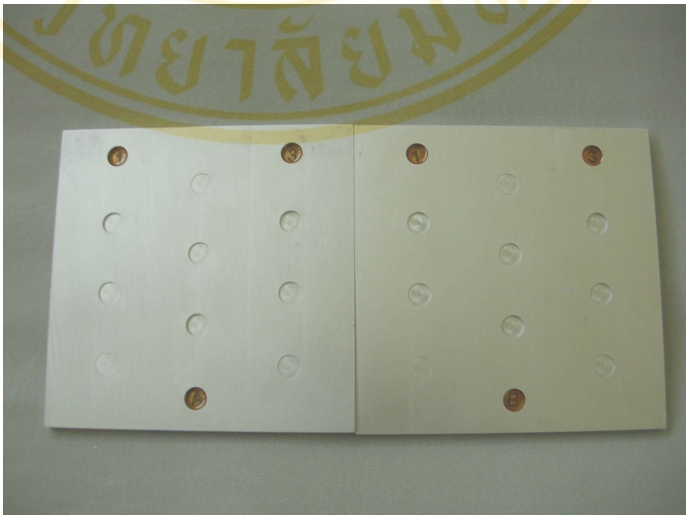

Figure 4 UAB phantom

Figure 5 Contrast detail phantom

Figure 6 Copper sheet (1.0 mmCu)

Figure 7 Line-pair test phantom

Figure 8 Anthropomorphic phantom

4.1.5 Image quality evaluators

The image quality evalutor was a qualified radiologist blinded to the experiments and a physicist with more than 5 years work experiences. The radiologist contributed to the clinical image quality evaluation.

4.2 Method

An experimental radiography was the major approach of the study entangled with structured assessment processes and observation of data collection. The methods applied for this study consisted of several different part, but most important methods in the experiment were divided into four successive stages of study with specific aim that was to assess physical and clinical performance characterization of Fuji XG1 Computed Radiography (CR) and X-ray machine used for the experiments underwent a Acceptance Testing and a quality control program (QCP), which was to assure their reliable capability in producing radiographs with optimum quality. This section will describe the Acceptance Testing and QCP and explain the sequence of the entire methods.

4.2.1 Quality Control Program of the X-ray machine and facilities

Basic tests of quality control were carried out during two weeks at the site of research study. Meanwhile, a daily program for checking readiness of the radiography facilities was done in parallel with the tests within the same period of the QCP. The tests were focused on an evaluation of the X-ray generator performances, which comprised of the tests, including the focal spots measurement, consistency of the tube current, the tube voltage accuracy and precision, the exposure time accuracy and precision, Half Value Layer (HVL) and the field indicator and light/X-ray alignments were tested to ensure the proper conditions.

The QC equipment used for the testing procedures have been calibrated routinely Department of at the SSDL, Science Ministry of Public Health. Thus, they were valid instruments for physical measurements to the X-ray system and its supports that were employed in the study.

All of the results of the QC test were interpreted and compared with respect to some reference standards that have been widely published by responsible international

organizations such as the American College of Radiology (ACR), The American Association of Physicists in Medicine (AAPM)[21] or the Institute of Physics and Engineering in Medicine (IPEM). Additionally, those standards have also been acknowledged to be a workable reference level in this country as well. Since then, the real performances of the CR were identified and verified.

4.2.2 Acceptance Testing of Computed Radiography Systems [22-23]

The Acceptance Testing was carried out during before the research study. The test protocol was based on AAPM TG-10. Meanwhile, a daily program for checking readiness of the radiography facilities was done in parallel with the tests within the same period of the QCP. The tests were focused on an evaluation of the Computed Radiography system, which comprised of the tests, including the system linearity, phosphor plat dark noise, cassette throughput, spatial resolution, low contrast sensitivity, laser beam function, wire mesh test and resolution uniformity across the receptor, distance accuracy measurements and thoroughness of erasure cycle.

4.2.2.1 Physical Inspection/Inventory

The process included checking all the components of the system against the purchase order and make sure that they were free from physical defects and properly installed.

4.2.2.2 System Linearity

The general purpose X-ray tube was raised until the focal spot was approximately 180 centimeter above the floor. The X-ray field light was activated and opens the collimator at 35 x 43 cm^2 cassette dimensions. Made an exposure at 80 kVp and low mAs, and read the exposure for 1 mR and 10 mR. Each image was evaluated and data were recorded for the sensitivity numbers and artifacts. Sensitivity number should be in the acceptable range.

4.2.2.3 Phosphor Plate Dark Noise

Imaging plates were erased by the 2nd erasure cycle to ensure removal of all residual signals from background radiation or other sources. After erasure, scanned several plates for image evaluation. Obvious artifacts, density shading, or uniformity presented on any output image. Corrective action was required before proceeding to other tests.

4.2.2.4 Cassette Throughput

Total of 6 loaded 35 x 43 cm^2 cassettes were processed for each specific cassette size as fast as possible. Start timing when the first cassette was loaded into the feed tray. The time was recorded when each Iimage plate was returned to its cassetts. The throughput for image plates 2 through 6 were calculated, starting with the time image plate number 1 was returned to its cassette, and ending with the return of image plate number 6 to its cassette. Throughput should be within 10% of the published specifications.

4.2.2.5 Spatial Resolution

Spatial resolution tests included measurement of the central and peripheral limiting resolution of each image, for each plate size and plate type. The resolution test phantom near parallel and near perpendicular to boath the x(row) and y(column) directions was placed in central areas of each cassette size. The cassette was exposed to a relatively low beam energy (approximately 60 kVp, 180 cm FID, and mAs to delivered 5 mR.The spatial resolution was about 10% of the manufacturer's specifications for either the vertical or horizontal directions.

4.2.2.6 Low Contrast Sensitivity/Detectability

Contrast resolution should be limited by quantum ststistics (x-rays absorbed in the imaging plate) in a well-designed system. The low contrast detectability phantom (UAB phantom, plate A and plate B) was placed on the cassette to be tested, and 1 mm copper to the collimator of the x-ray system, completely intercepting the beam. A radiographic technique of 80 kVp, 180 cm FID and mAs to deliver incident

exposures of 1.0 mR and 5 mR to imaging plate was employed. Contrast sensitivity shoud improved with increased exposure, relate to reduced quantum noise.

4.2.2.7 Laser Beam Function

Laser beam scan line integrity, beam jitter, signal dropout, and focus were evaluated in this test. Used of a radiographic technique of 80 kVp, 180 cm FID and mAs to deliver an incident exposure of 5 mR. The steel straight edge was placed on a 35 x 43 cm^2 centered on the cassette and roughly perpendicular to the laser beam scan lines. Laser beam jitter was evaluated by examining the edge of the ruler on the image. Ruler edges should be straight and continuous over the full length of the image.

4.2.2.8 Wire Mesh Test

This test utilized a screen-film contect test tool to verified focus over the total field of view of the phosphor receptor. The wire mesh test tool was placed in direct contact with the PSP cassette, and exposed the imaging plate to a relatively low beam energy, 60 kVp, 180 cm FID, and mAs to deliver 5 mR. The resultant image should be distortion free and sharp over the whole field of view.

4.2.2.9 Distance Accuracy Measurements

Distance accuracy was determined from a known sized object, the image reduction factor, and the measured distance on the image.Several known square of high contrast was palced around the periphery of an image Plate. Using a standard radiographic technique exposed the plate to 1 mR. Measured the resultant aspect ratio of the imaged objects with the digital calipers on the display workstation. Verified that the x and y distance are within 2% of the absolute distance.

4.2.2.10 Accuracy/Thoroughness of erasure cycle

The erasure capability was test, exposed a PSP screen to an incident exposure of 50 mR (80 kVp, 25 mAs, 180 cm., no filtration) with a centrally placed high contrast test object in contact. The plate was processed and requested for return of the specific plate for those systems with internal stackers. Re-exposed the plate to a

uniform incident exposure of about 1 mR (80 kVp, 0.5 mAs, 180 cm.) With a slightly smaller collimated area, and processed using the same readout algorithm. Verification for lack of residual signal from the previous high exposure by looking for a ghost image of the resolution test pattern was performed.

4.2.3 Physical and clinical performance characterization of a computed radiography system

4.2.3.1 High contrast resolution

This test should be done for each size of the image plates (35x43 cm^2 , 35x35 cm^2 , and 18x24 cm^2). Use a 60 kVp unfiltered x-ray beam (FID = 180 cm). Placed line-pair test pattern devices on the image plate (scan and sub-scan direction). Exposed the plate with an exposure of about 5.0 mR. Processed the plate, Set the window and level to optimally visualize the line-pair patterns using 2-3x magnification. The limiting resolution should be within 10% of the expected value in both the scan and sub-scan direction.

4.2.3.2 Low-contrast Detectability

This test should be done for UAB contrast resolution test tools and contrast-detail phantom. UAB phantom consist of 6.1-mm-thick alloy aluminum target plates with each plate having a gradation of 1.1-cm-diam circular attenuation differences or holes.[16] An 80 kVp beam was used with 1 mmCu (FID = 180 cm). For each plate, the image of phantom using 0.5, 0.6, 0.7, 0.8, 0.9, 1.0, 2.0, …, 6.0 mR exposures to the plates were acquired. A constant delay time of 10 minutes before reading each of the plates was employed. Each time read the plate using TEST, CONTRAST body part, set the window and level to optimally.

The contrast-detail phantom utilized in this study was custom mode. The phantom was constructed on a 0.5 cm thick acrilic plastic sheet with 30 x 30 cm^2 area size. Holes of varing diameters and depths were drilled into the acrilic plastic sheet, 14x15 holes, for a total of 210. The holes in one direction had a constant diameter but decreasing depth (therefore, decreasing contrast on the image). The holes in the other direction had a constant depth (therefore, same contrast on the image) but decreasing

diameter. The target diameter ranged from 1.0 to 8.0 mm and target depth ranged from 0.5 to 7.0 mm. The x-ray focal to image recepter distance (FID) was initially set at 180 cm with the 1 mmCu added. The kVp setting at 80 kVp and mAs settings varied for 0.5, 0.6, 0.7, 0.8, 0.9, 1.0, 2.0, …, 6.0 mR.

4.2.3.3 Modulation Transfer Function (MTF)

Images were acquired by a line-pair test pattern. The device was positioned both vertically and horizontally on each plate to acquire data for the MTF along the scan and sub-scan directions of laser read out. The line-pair obtained from each projection provided optimum sampling of the line spread function (LSF). The x-ray resolution test pattern radiograph measurements were made using 60 kVp, FID 180 cm for each plate size (35x43 cm^2, 35x35 cm^2 , and 18x24 cm^2). Acquied image will be analyzed to find out MTF by imageJ program.

4.2.3.4 Clinical performance characterization

Images obtained from various anthropomorphic phantoms were acquired with various anatomical sites and view (e.g. skull AP axial, lateral skull, chest PA, etc.) Exposure factors were based on the appropriate prescribed anatomical menus of the system. The appearance of CR images varied as a function of radiographic technique exposure (Entrance Skin Air Kerma, ESAK). A radiologist blinded to the experiment was requested to evaluate clinical quality of images based on criteria described in table 3.

Measurements of the ESAK values were based on estimation from the free-in-air exposure measurements. Therefore, some of the related ESAK parameters such as the Focal-Chamber-Distance (FCD) as well as the distance to entrance point (FED) for all type of examinations were recorded accordingly. The figure 7 below portrayed the geometry used for the measurement of the ESAK.

The levels of patient radiation dose introduced the use of guidance levels as an efficient standard for optimising the radiation protection of a typical adult patients. The physical parameter recommended for monitoring guidance levels the in conventional radiography was the entrance skin dose (ESD), is presented in table 1.

Table 1 Diagnostic Radiography ESD BSS Guidance Levels [24]

Examination	Entrance dose (mGy)
Skull AP/PA	5.00
Skull LAT	3.00
Chest PA	0.40
Chest LAT	1.50
Thoracic spine AP	7.00
Thoracic spine LAT	20.00
Lumbar spine AP	10.00
Lumbar spine LAT	30.00
Abdomen AP	10.00
Pelvis AP	10.00

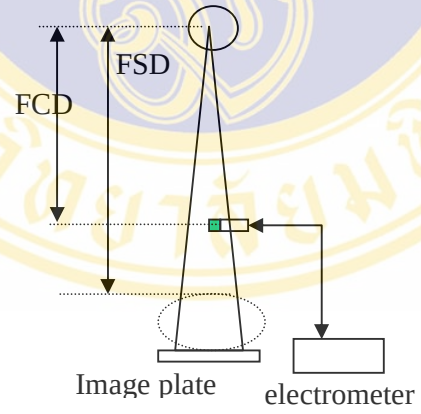

Figure 9 The geometry for the free-in-air measurements

The measured ESE at the surface areas was estimated using the following equation :[5]

Exposure @ surface = mR/mAs x $(FCD/FSD)^2$ x mAs_1 where,

mR/mAs = the estimated exposure values (free-in-air)
FCD = the Focal-Chamber-Distance
FSD = the Focal-Skin-Distance
mAs_1 = the reading mAs values with respect to each examination

The measured ESE may be expressed in various levels of the exposure dose that specific to the position.

The following table 2 presented preliminary technical data sets containing information about parameters that were plunged into the evaluation process. [25-26] ESAK was then calculated by factor 0.00876 multiply with Entrance Skin Exposure.

Table 2 The parameter setting for various anthropomorphic phantoms

ROI / VIEW	parameter	
	kVp	mAs
1. skull : AP	75	24.90
	75	28.00
	75	31.00
	75	35.00
	75	37.50
2. skull : lateral	70	15.00
	70	16.50
	70	19.00
	70	20.50
	70	23.00
3.chest PA	105	2.50
	105	3.00
	105	3.50
	105	4.00
	105	5.00

Table 2 The parameter setting for various anthropomorphic phantoms (Continued)

ROI / VIEW	parameter	
	kVp	mAs
4. Chest lateral	110	16.30
	110	18.00
	110	20.30
	110	23.00
	110	25.00
5. thoracic spine : AP	75	14.40
	75	16.00
	75	18.00
	75	20.00
	75	22.00
6. thoracic spine :Lateral	80	21.40
	80	24.00
	80	27.20
	80	30.40
	80	32.00
7. lumbar spine : AP	70	18.80
	70	21.20
	70	22.80
	70	25.20
	70	26.80
8. lumbar spine : Lateral	85	27.80
	85	32.00
	85	34.60
	85	37.80
	85	40.60
9. hand : PA	50	1.80
	50	2.40
	50	3.00
	50	3.80
	50	4.10

Table 2 The parameter setting for various anthropomorphic phantoms (Continued)

ROI / VIEW	parameter	
	kVp	mAs
10. hand : oblique	50	3.00
	50	3.80
	50	4.10
	50	4.80
	50	6.00
11. knee joint : AP	55	3.50
	55	4.10
	55	4.50
	55	4.90
	55	5.40
12. knee joint : Lateral	55	3.50
	55	3.80
	55	4.10
	55	4.50
	55	4.90
13. lower leg AP	60	10.90
	60	12.00
	60	13.10
	60	15.00
	60	17.00
14. lower leg : lateral	60	10.90
	60	12.00
	60	13.10
	60	15.00
	60	17.00
15. foot : PA	50	1.80
	50	2.40
	50	3.00
	50	3.80
	50	4.10

Table 2 The parameter setting for various anthropomorphic phantoms (Continued)

ROI / VIEW	parameter	
	kVp	mAs
16. foot : oblique	50	1.80
	50	2.40
	50	3.00
	50	3.80
	50	4.10
17. Pelvic AP	70	20.00
	70	22.80
	70	24.80
	70	27.20
	70	30.00

4.2.4 Image quality evaluation

The clinical aspects of image quality were reviewed independently, using rather specific tools that have been documented as the checklists. Scoring systems were applied for quantitative measurement upon the both aspects of image quality. In case of the scoring systems, the image quality descriptors were employed and defined as composite indexes, reflecting overall fulfillments of the clinical quality aspects about the radiographs that have been undergoing such evaluation.

The clinical quality criteria are presented in table 3.[27-28] In addition to that, an additional list that contained information about clinical quality discrepancy in the phantom imaging was also defined as was highlighted in table 4.

Table 3 The clinical quality criteria for various anthropomorphic phantoms

The skull radiograph
1. Antero-posterior view
a) Synmetric projection of the skull, particularly cranial vault, orbits and petrous bones b) The apex of the petrous temporal bone is projected into the center of orbit c) The outer and inner lamina of the cranial vault d) The fronal sinuses
2. Lateral view
a) The outer and inner lamina of the cranial vault b) The apex of the petrous temporal bone c) The vertex of the skull and the trabecular structure or the cranium d) Superimposition of the mandibular angles and ascending rami
The chest-lung and heart radiograph
3. Postero-anterior view
a) Symmetric projection of the thorax as shown by central postion of the spinous process between the medial ends of the calvicles b) The whole cage above the diaphragm c) The vascular pattern in the whole lungs particularly the peripheral vessels e) The trachea andproximal bronchi, the border of the heart and aorta f) Visualization of the retro cardia lung and the mediastinum

Table 3 The clinical quality criteria for various anthropomorphic phantoms (Continued)

4. Lateral view
a) The apex of lungs should be seen clear of the arm/shoulder shadows b) The costo-phrenic angles c) The psoterior border of the heart, mediastinum, diaphragm, sternum and thoracic spine
The thoraic spine
5. Antero-posterior view
a) Demonstration all of the twelve vertebrae b) The Vertebral alignment c) Transverse process, Spinous process d) Intervertebral disk space
6. Lateral view
a) The vertebrae clearly seen through rib and lun shadows b) No patient rotation indicated by the ribs superimposed posteriorly c) The vertebral alignment d) Spinous proces e) Intervertebral foramina, superimposed f) Intervertebral disk space
The lumbar spine
7. Antero-posterior view
a) The uppoer and lower plate surfaces in the centered beam area b) The spinous and transverse process c) The cortex and trabecular structures d) The sacro-iliac joints e) The vertebral alignment f) Intervertebral disk space

Table 3 The clinical quality criteria for various anthropomorphic phantoms (Continued)

8. Lateral view
a) As a single line, of the upper and lower-plate surfaces with resultant visualization of the intervertebral spaces b) Totally superimposition of the posterior vertebral edges c) The spinous processes d) The cortex and trabecular structures e) The central spinal canals f) The intervertebral joints particularly the facet joints g) The vertebral alignment
The hand
9. Postero-anterior view
a) The hand with no rotation, which is in true PA or AP position b) Slightly seperated digits with no soft tissue overlap c) All anatomy distal to the radius and ulna, including the joints, bonny alignments, trabecular petterns and the soft tissue contour
10. Oblique view
a) Minimal overlap of the third-fourth and fourth-fifth metcarpal shafts b) Slight overlap of the metcarpal bases and heads c) Seperation of the second and third metacarpals d) The soft tissue contour and bonny trabeculation
The knee joint
11. Antero-posterior view
a) The femorotibial joint space is shownm including the medial and lateral compartments of the distal femur b) The knee is seen fully extended and soft tissue around the knee joint c) The interspaces should be demostrate equally in width on both sides d) The patella completely superimposed on the femur e) Bonny detail surrounding the patella on the distal demur

Table 3 The clinical quality criteria for various anthropomorphic phantoms (Continued)

12. Lateral view

a) The joint space between femoral condyles and tibia
b) The patella is shown in the lateral profile
c) The flexition of the knee is seen approximately 60 degrees
d) All soft tissue around the knee joint
e) Proper density on the femoral condyles

The tibia and fibula bones

13. Antero-posterior view

a) The ankle and knee joints without rotation
b) The proximal and distal articulations of tibia and fibula with moderately overlapping
c) Trabecular detail and soft tissue for the entire leg

14. Leteral view

a) The distal fibula lying over the posterior half of the tibia
b) Almost overlap of the tibia on the proximal fibular head
c) No superimposition of femoral condyles due to the divergence of the beam
d) Almost separation of the tibial and fibular bodies (shafts) except at their articular ends
e) Trabecular detail and soft tissue

The foot

15. Postero-anterior view

a) An equal amount of psace betwee the adjacent mid-shaft of the second through fourth metatarsal bases
b) Overlapped of the second through fifth metatarsal bases
c) The joint spaces
d) The bonny contour and trabecualation
e) The soft tissues

Table 3 The clinical quality criteria for various anthropomorphic phantoms (Continued)

16. Oblique view
a) The third through fifth tarsal bases free of superimposition b) The leteral tarsals are shown with less superimpostion than in the AP projection c) The lateral tarsometatarsal and intertarsal joints d) The tuberosity of the fifth metatarsal e) The space between the shaft of the second through fifth metatarsal is seen in equidistance f) Suffeicient density of the phalanges, metatarsals, and tarsals g) The soft tissuers
The pelvic bones
17. Antero-posterior view
a) The pubic and ischial rami b) The sacrum and its intervertebral foramina c) The sacro-iliac joints d) The neck of the femora which should not be distorted by shortening or rotation e) The spongiosa and corticalis, and of the trochanters f) Both acetabuli

Table 4 An additional list of the clinical criteria discrepancy in the phantom radiography

Position	Remarks
Skull Lateral	- The sella floor is poorly shaped and not clearly seen
Postero-anterior Chest	- No full inspiration - The lung area is still obscured by the medial border of the scapulae - There is no air filling in the trachea

Table 4 An additional list of the clinical criteria discrepancy in the phantom radiography (Continued)

Position	Remarks
	- There is angiogram of the heart - The lungs area is seen to be pneumothorax
Lateral Chest	- No full inspiration - No air filling in trachea - The apex lung can't be seen free of the shoulder shadows
Antero-posterior T-spine	- A slight rotation deviation appears between the thoracic spine 8 and 10
Antero-posterior L-spine	- Science the lumbar spine is built in apart of the pelvis, which is symmetric, the sacroiliac joints are seen partially - The psoas shadows can't possibly be seen in this phantom model
Antero-posterior Pelvis	- The phantom model presented asymmetric design of pelvic bones - There is pubic separation in this phantom model
Antero-posterior knee joint	- The patella is too obvious seen than normal anatomy
Lateral knee joint	- The patella is too much superimposed to anterior border of the femoral condyle - The patello-femoral space

In the checklists, each list composed of the statements elaborating the clinical quality criteria that critically required for each organ/view of an evaluated radiograph. Therefore, the number of statements for each individual checklist was various. Additionally, choosing one of the optional marks available in the checklist to which evaluated statement such as “yes” or “no” was very convenient for knowing its fulfillment, whereby, a score with the value of one was necessarily given to that the mark “yes” while the score of zero was applied to the mark “no”. An equation was employed in the calculation of the composite index for clinical image quality fulfilled, the so-called the CQCI. The equation was expressed as the following, [29]

$$CQCI = \frac{\text{Number of criteria fulfilled}}{\text{Total number of criteria}}$$

Where, CQCI = the composite index of clinical quality criteria

$(0 \leq CQCI \leq 1)$

Tough the calculated CQCI values possible ranged from 0 to 1, the indexes that equal to 1 denoted the maximum fulfillment of all critical criteria and become the prerequisite value for passing the evaluated clinical aspects.

CHAPTER 5
RESULTS AND DISCUSSIONS

5.1 Acceptance Testing of Computed Radiography System

Table 5 tabulates the result of the system in regards of physical inspection, system linearity, phosphor plate dark noise, cassette throughput, spatial resolution, low contrast detectability, laser beam function, wire mesh test, distance accuracy measurements, accuracy/thoroughness of erasure cycle.

Table 5 Result of Acceptance test for Fuji XG1 Computed Radiography

Test of performance	Result
Physical inspection	Free from physical defects and properly installed
System linearity	Sensitivity number at 1 mR was 187 and the sensitivity number at 10 mR was 19. The sensitivity number are in acceptable range.
Phosphor plate dark noise	The acquied image was the uniform image without any artifacts.
Cassette throughput	The processing capacity of the cassettes (35 x 43 cm^2) was approximate 80 Ips/hr which the procesing capacity of the manufacturer's specifications is approximate 54 Ips/hr. The cassette throughput are in acceptable.
Spatial resolution	The lp/mm was 2.2 of 35 x 43 cm^2 image plate, 2.2 lp/mm of 35 x35 cm^2 image plate and 2.5 lp/mm of 18 x 24 cm^2 image plate.
Low contrast detecability	The percent contrast of the exposure at 1.0 mR was 3.28 and 5 mR was 2.19. The low contrast detectability are lower proportionately at higher exposure.
Laser beam function	The ruler edges was straight and continuous without any undershoot or overshoot of the scan lines in light to dark transitions.

Table 5 Result of Acceptance test for Fuji XG1 Computed Radiography (Continued)

Test of performance	Result
Wire mesh test	The image was distortion free and sharp over the whole field of view.
Distance accuracy measurement	The imaged objects with the digital calipers on a display workstation and the known sized object was much lesser than that from the accptance limit (the x and y distance are within 2% of the absolute distance.

Result shows acceptable quality of installation of the Fuji XG-1 CR system.

5.2 Physical and clinical performance characterization of a computed radiography system

5.2.1. Spatial resolution

Spatial resolution testing was performed on computed radiography using a Fuji FCR XG1 plate reader and a PACS workstation. Acquired image is presented in Figure 10. The limiting spatial resolution and observed resolution for the FCR XG1 are presented in table 6.

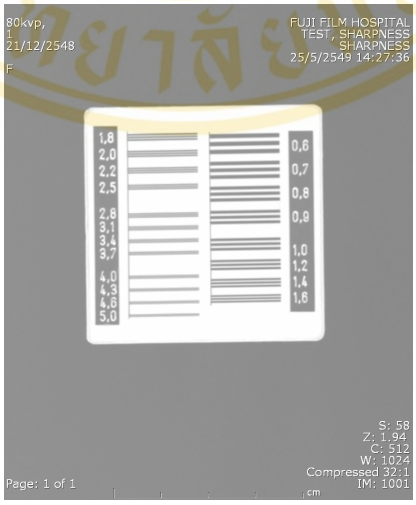

Figure 10 Image of resolution test pattern

Table 6 The limiting spatial resolution and observed resolution for the FCR XG1

Image Plate (cmxcm)	Scan Direction	Limiting Resolution(lp/mm)	Observed Resolution (lp/mm)
35 x 43	scan	2.5	2.2
	sub-scan	2.5	2.2
35 x35	scan	2.5	2.2
	sub-scan	2.5	2.2
18 x 24	scan	5.0	2.5
	sub-scan	5.0	2.5

From table 6, results show that observed spatial resolution obtained from scan and sub-scan direction for different IP sizes deviate more than 10% of the specification. This may be due to the optimal imaging condition set during the experiment differed from specified conditions required by the manufacturer.

The quality control program is a vital portion of everyday CR operation and imaging. The high contrast (spatial) resolution testing is well outlined to set limits on the limiting resolution for the scan (horizontal) and sub-scan (vertical) directions that will provide the best results for that CR equipment. The high contrast square wave resolution pattern provides an effortless way of testing for the spatial resolution of CR equipment. Using this tool for quality assuarance will help the medical physicist determine the need for corrective actions hopefully at an early stage in the degradation of the resolution of the equipment.

Some of the downfalls of using the line pair test to measure the limiting spatial resolution of the computed radiography is that at times there can be a missalignment error and it is not always an accurate representation of the computed radiography machine. The main downfall is that the line-pair test pattern does not always accurately represent the limiting resolution of the computed radiography machine due to the discrete frequencies of the line-pair test pattern. When the image must be leveled and displayed in the zoom position this can cause misinterpretations or inaccuracies in the observed resolution.

The exposure factors along with focal spot size selection are also crucial for this procedure. Selecting different focal spot sizes will result in different levels of spatial resolution.

Spatial resolution testing is critical due to necessity of the high image quality. It is important in digital x-ray systems to determine the optimal balance of pixel size and noise.

5.2.2. Low Contrast Detectability

Acquired image is presented in figure 11.Percent contrast for UAB phantom imaged with 1 mmCu attenuator, which represents small size patient, is presented in figure 12. The exposure to the CR plates was set at eleven different value, 0.5, 0.6, 0.7, 0.8, 0.9, 1.0, 2.0, 3.0, 4.0, 5.0 and 6.0 mR. The %contrast between 2.19-3.83. Result showed that as the exposure to the CR plates increased, the percent contrast decreased. This means the improvement of low contrast visibility can be improved by increasing amount of radiation given to the IP. There was no difference between % contrast detectability observed from the given exposure between 2-4 mR. This implies that radiation dose to patient can be optimized at exposure level of 2 mR exit exposure to the IP.

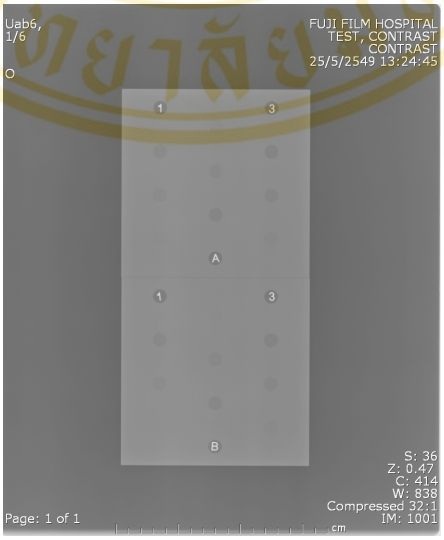

Figure 11 Image of UAB Phantom

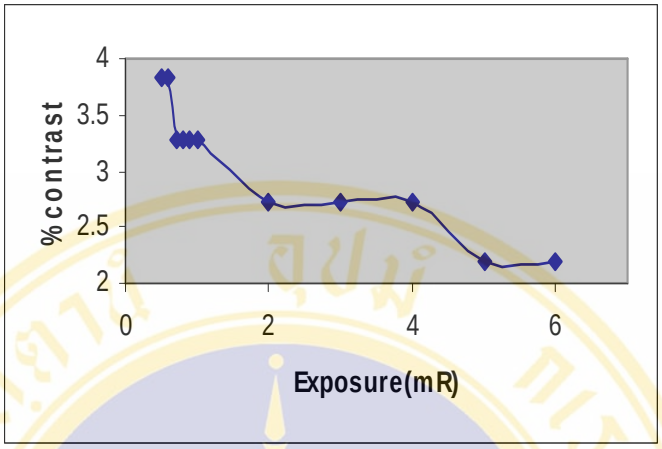

Figure 12 Percent contrast of UAB phantom related to exposure (mR)

Image of Contrast detail phantom shown in figure 13. Detection ratio, R was calculated by n/210, where n was the number of the detected targets assessed by the observer and 210 was the total number of targets on the phantom. Figured 14 shows the detection ratio obtained from images with contrast-detail phantom. The exposure to the CR plates was set at eleven different values, 0.5, 0.6, 0.7, 0.8, 0.9, 1.0, 2.0, 3.0, 4.0, 5.0 and 6.0 mR. The detection ratio between 0.8238 - 0.8857. As the exposure to the CR plates increased, the detection ratio increased.

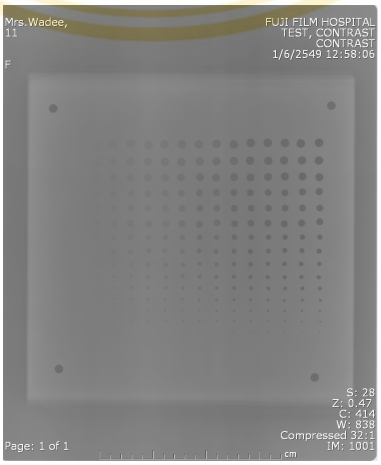

Figure 13 Image of Contrast detail phantom

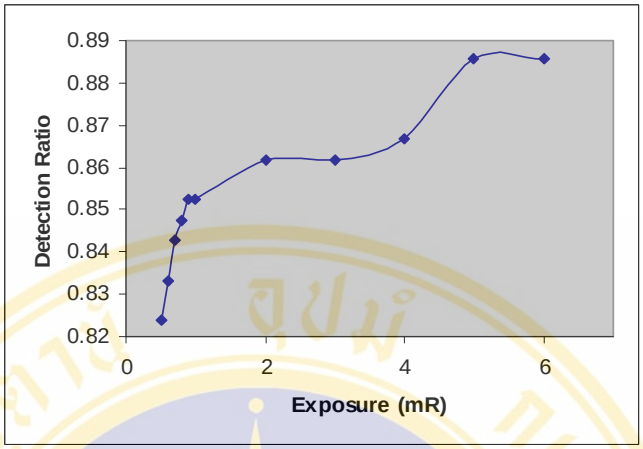

Figure 14 Detection ratio of contrast detail phantom

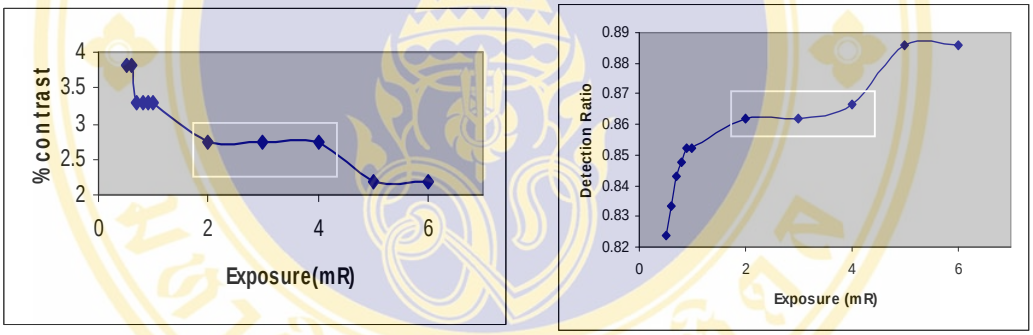

Figure 15 Comparison between %contrast of UAB phantom and detection ratio of contrast detail phantom

Figure 15 show Comparison between %contrast of UAB phantom and detectionratio of contrast detail phantom. The result correlates well with low contrast detectability method using UAB phantom. The radiation exposure increases, the contrast detail detectability can be improved. The result also showed that optimized exit exposure to the IP is 2 mR.

The fact that threshold contrast was found to vary from image noise level (i.e., with input phosphor exposure rate and with the degree of digital noise reduction), indicates that results obtained with the test object are sensitive to typical variations in image quality. Also of practical importance is that threshold contrast was found to be

independent of exposure values. This observation can be explained by the fact that threshold contrast is primarily dependent on image noise.

5.2.3. Modolation Transfer Function (MTF)

Modulation Transfer Function at 20% (20%MTF) was used as an indicator for systemic spatial resolution in this study. When varying scanning imaging plate, there was little difference in spatial resolution observed. The ranges of 20% MTF of all imaging plate were 1.65-2.25 lp/mm are presented in table 7. Figure 16-21 show the measured MTF in the scan and sub-scan directions for 35 x 43 cm^2, 35 x 35 cm^2 and 18 x 24 cm^2 image plates.

Table 7 20%MTF in scan and sub-scan direction of 35 x 43 cm^2, 35 x 35 cm^2 and 18 x 24 cm^2 image plates.

Image Plates	Spatial frequency (lp/mm)	
	Scan	Sub-Scan
35 x 43 cm^2	1.65	1.91
35 x 35 cm^2	1.69	1.91
18 x 24 cm^2	2.25	2.17

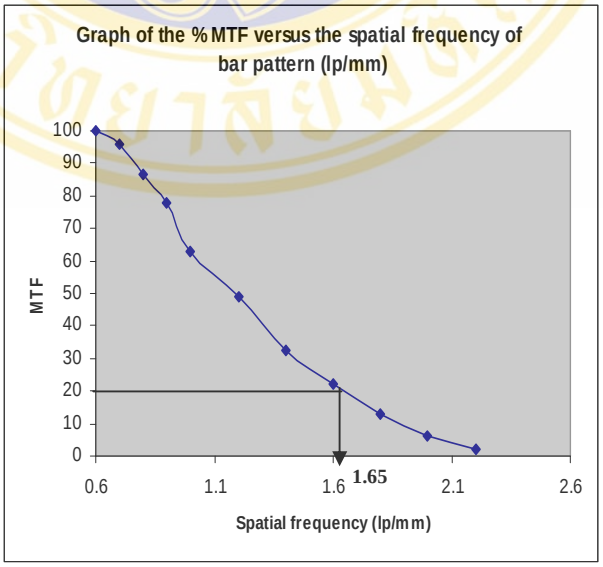

Figure 16 Graph shows spatial resolution at 20% MTF with scan direction for 35 x 43 cm^2 image plate

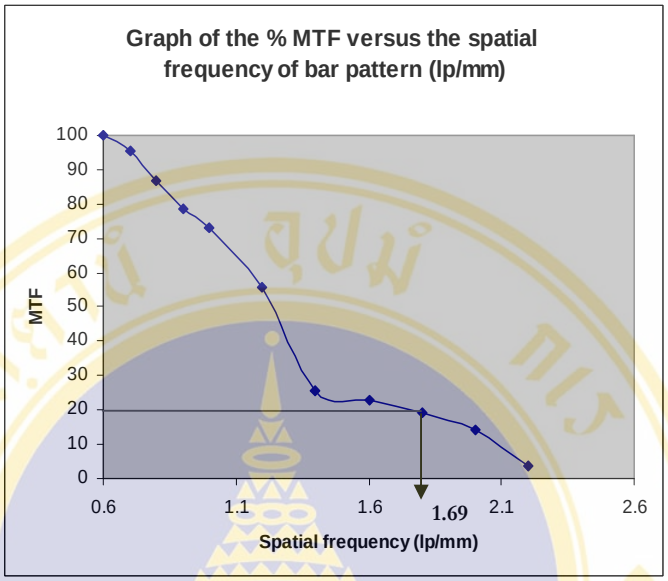

Figure 17 Graph shows spatial resolution at 20% MTF with scan direction for 35 x 35 cm^2 image plate

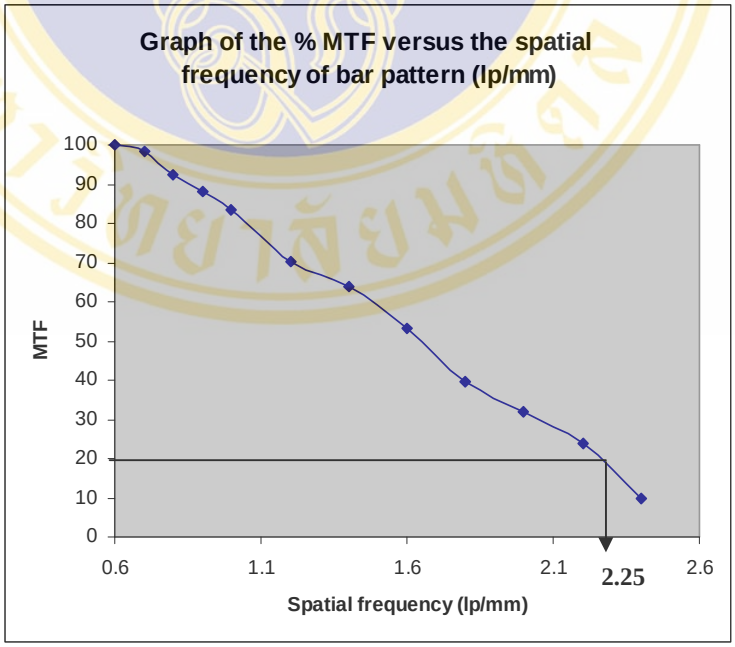

Figure 18 Graph shows spatial resolution at 20% MTF with scan direction for 18 x 24 cm^2 image plate

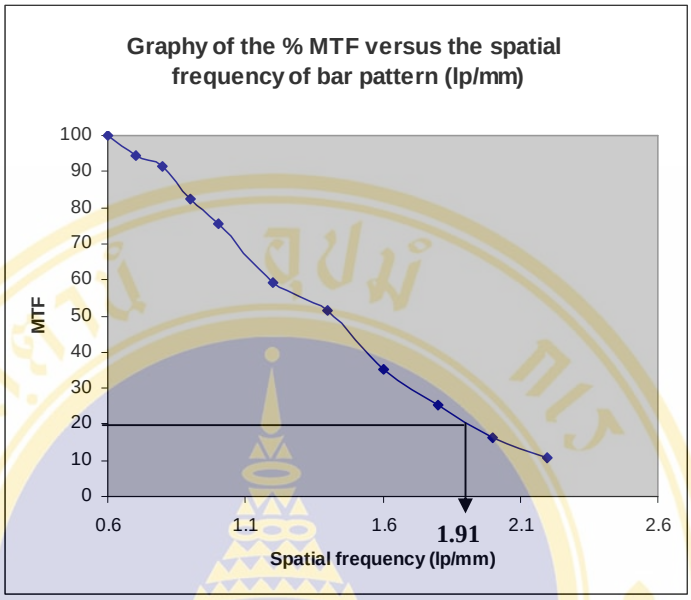

Figure 19 Graph shows spatial resolution at 20% MTF with sub - scan direction for 35 x 43 cm^2 image plate

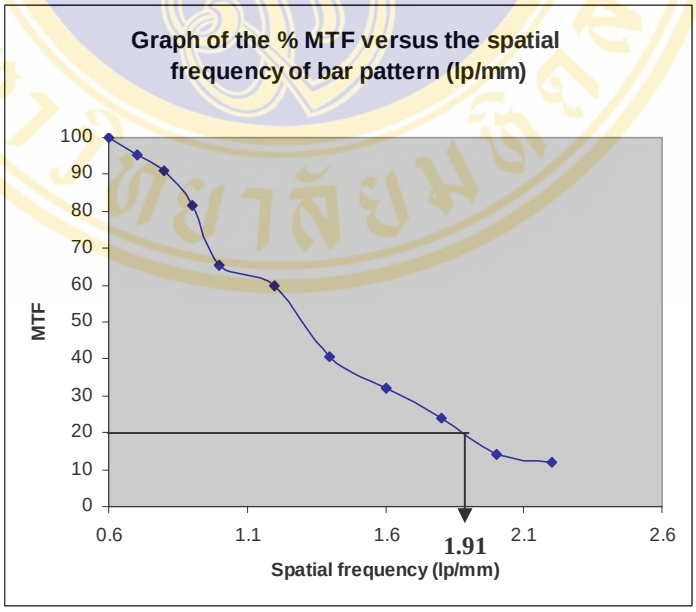

Figure 20 Graph shows spatial resolution at 20% MTF with sub - scan direction for 35 x 35 cm^2 image plate

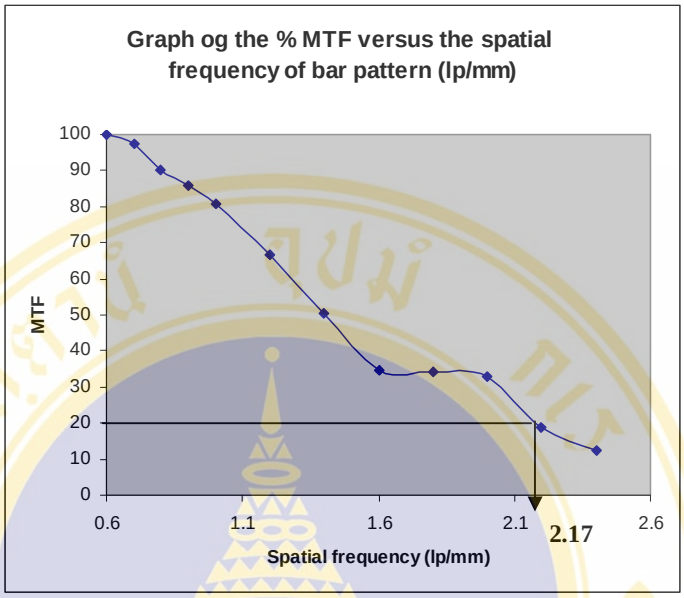

Figure 21 Graph shows spatial resolution at 20% MTF with sub - scan direction for 18 x 24 cm^2 image plate

The main goal of these MTF measurements was neither the evaluation nor the comparision of the performance of digital radiographic system, but rather the quality control of the reproducibility of the spatial resolution measurement.

The results showed that small image plate of size 18 x 24 cm^2 provides best spatial frequency response as compared to bigger size image plate (35 x 43 cm^2 and 35 x 35 cm^2) in both scan directions. Regarding effects of scan direction, MTF from the sub-scan direction were superior than the scan direction in big size IP (35 x 43 cm^2 and 35 x 35 cm^2). In small IP (18 x 24 cm^2), different scan directions do not provides significant differences in MTF. This may be due to limitation in Nyquist frequency requirements from the laser scan frequency.

5.2.4. Clinical image quality

5.2.4.1. Radiation Exposure (ESAK)

In this study, clinical image quality was evaluated based on radiographic images taken by different variable exposure techniques from standard technical parameters used in clinical settings. The use of mAs settings between ± 10% and ± 20% of standard technical parameter for 4 values and kVp selections between 50 kVp and 110 kVp sufficiently provided optimum clinical image quality results. The following table 8 presents ESAK data obtained from various exposure techniques.

Table 8 The parameter setting for various anthropomorphic phantoms

ROI / VIEW	parameter			
	kVp	mAs	ESE(mR)	ESAK(mGy)
1. skull : AP	75	24.90	188.74	1.65
	75	28.00	212.30	1.86
	75	31.00	235.05	2.06
	75	35.00	265.37	2.32
	75	37.50	284.33	2.49
2. skull : lateral	70	15.00	86.51	0.76
	70	16.50	95.16	0.83
	70	19.00	109.58	0.96
	70	20.50	118.23	1.04
	70	23.00	132.65	1.16
3.chest PA	105	2.50	7.59	0.07
	105	3.00	9.11	0.08
	105	3.50	10.63	0.09
	105	4.00	12.15	0.11
	105	5.00	15.19	0.13
4. Chest lateral	110	16.30	59.98	0.53
	110	18.00	66.24	0.58
	110	20.30	74.70	0.65
	110	23.00	84.64	0.74
	110	25.00	92.00	0.81

Table 8 The parameter setting for various anthropomorphic phantoms (Continued)

ROI / VIEW	parameter			
	kVp	mAs	ESE(mR)	ESAK(mGy)
5. thoracic spine : AP	75	14.40	115.41	1.01
	75	16.00	128.24	1.12
	75	18.00	144.26	1.26
	75	20.00	160.29	1.40
	75	22.00	176.32	1.54
6. thoracic spine :Lateral	80	21.40	247.60	2.17
	80	24.00	277.68	2.43
	80	27.20	314.70	2.76
	80	30.40	351.73	3.08
	80	32.00	370.24	3.24
7. lumbar spine : AP	70	18.80	130.84	1.15
	70	21.20	147.55	1.29
	70	22.80	158.68	1.39
	70	25.20	175.38	1.54
	70	26.80	186.52	1.63
8. lumbar spine : Lateral	85	27.80	313.05	2.74
	85	32.00	360.35	3.16
	85	34.60	389.63	3.41
	85	37.80	425.66	3.73
	85	40.60	457.19	4.01
9. hand : PA	50	1.80	3.14	0.03
	50	2.40	4.18	0.04
	50	3.00	5.23	0.05
	50	3.80	6.62	0.06
	50	4.10	7.15	0.06
10. hand : oblique	50	3.00	5.46	0.05
	50	3.80	6.91	0.06
	50	4.10	7.46	0.07
	50	4.80	8.73	0.08
	50	6.00	10.91	0.10

Table 8 The parameter setting for various anthropomorphic phantoms (Continued)

ROI / VIEW	parameter			
	kVp	mAs	ESE(mR)	ESAK(mGy)
11. knee joint : AP	55	3.50	9.31	0.08
	55	4.10	10.91	0.10
	55	4.50	11.97	0.10
	55	4.90	13.04	0.11
	55	5.40	14.37	0.13
12. knee joint : Lateral	55	3.50	8.70	0.08
	55	3.80	9.45	0.08
	55	4.10	10.19	0.09
	55	4.50	11.19	0.10
	55	4.90	12.18	0.11
13. lower leg AP	60	10.90	33.98	0.30
	60	12.00	37.41	0.33
	60	13.10	40.84	0.36
	60	15.00	46.77	0.41
	60	17.00	53.00	0.46
14. lower leg : lateral	60	10.90	33.98	0.30
	60	12.00	37.41	0.33
	60	13.10	40.84	0.36
	60	15.00	46.77	0.41
	60	17.00	53.00	0.46
15. foot : PA	50	1.80	3.20	0.03
	50	2.40	4.27	0.04
	50	3.00	5.34	0.05
	50	3.80	6.76	0.06
	50	4.10	7.30	0.06
16. foot : oblique	50	1.80	3.20	0.03
	50	2.40	4.27	0.04
	50	3.00	5.34	0.05
	50	3.80	6.76	0.06
	50	4.10	7.30	0.06

Table 8 The parameter setting for various anthropomorphic phantoms (Continued)

ROI / VIEW	parameter			
	kVp	mAs	ESE(mR)	ESAK(mGy)
17. Pelvic AP	70	20.00	139.19	1.22
	70	22.80	158.68	1.39
	70	24.80	172.60	1.51
	70	27.20	189.30	1.66
	70	30.00	208.79	1.83

The results showed that ESAK values obtained from all radiographic examination were under IAEA BSS guidance levels.

5.2.4.2. Clinical performance characterization

The result of the clinical quality criteria, the 17 sets of clinical quality criteria were diagnostically defined as critical aspects with respect to the phantom radiographs. The radiographs were shown in figure 22-38. For some cases, number of clinical checkpoints had to be justified or reduced since they appeared different from the usual anatomical features in the normal radiographs.

(a) (b) (c)

Figure 22 Picture of Skull AP (a) 24.9 mAs (b) 28.0 mAs (c) 31.0 mAs (d) 35.0 mAs (e) 37.5 mAs

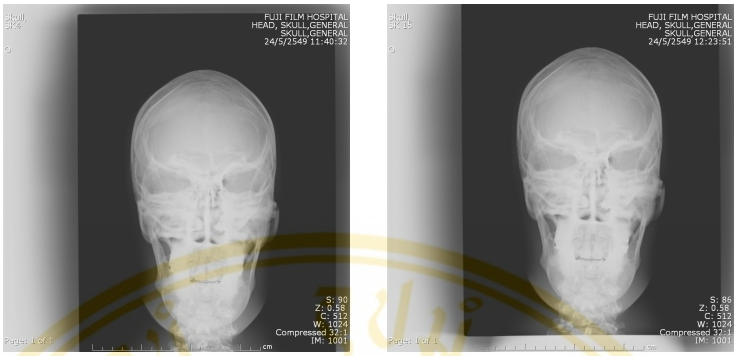

(d) (e)

Figure 22 Picture of Skull AP (a) 24.9 mAs (b) 28.0 mAs (c) 31.0 mAs (d) 35.0 mAs (e) 37.5 mAs (Continued)

(a) (b) (c)

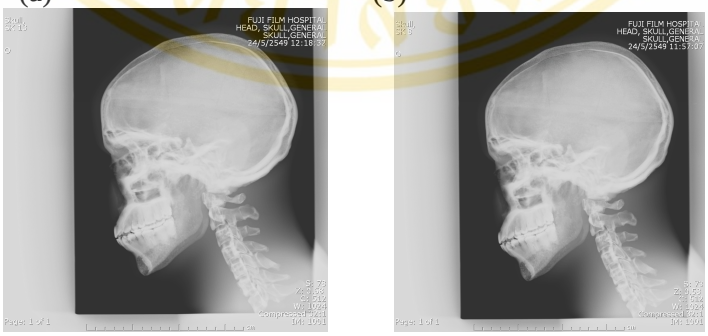

(d) (e)

Figure 23 Picture of Skull lateral (a) 15.0 mAs (b) 16.5 mAs (c) 19.0 mAs (d) 20.5 mAs (e) 23.0 mAs

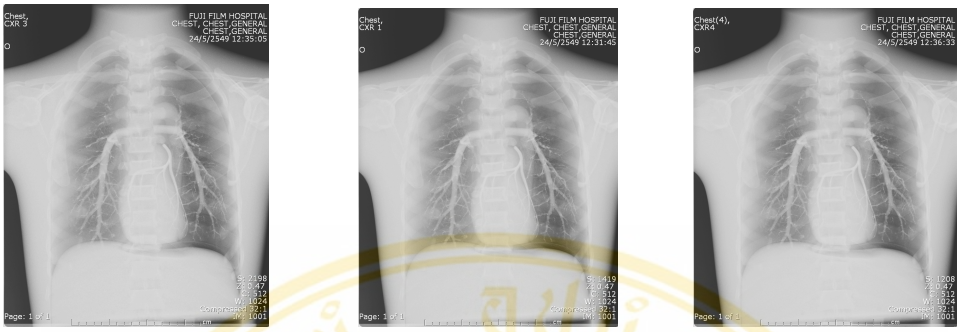

(a) (b) (c)

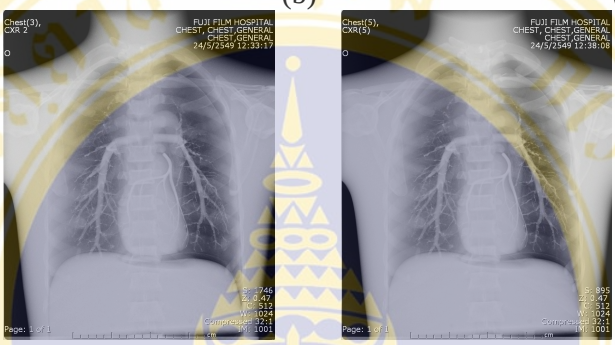

(d) (e)

Figure 24 Picture of Chest PA (a) 2.5 mAs (b) 3.0 mAs (c) 3.5 mAs (d) 4.0 mAs (e) 5.0 mAs

(a) (b) (c)

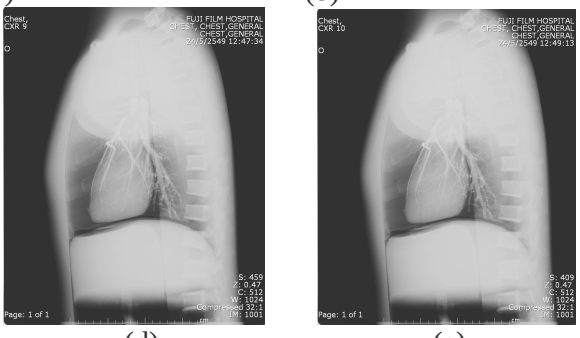

(d) (e)

Figure 25 Picture of Chest lateral PA (a) 16.3 mAs (b) 18.0 mAs (c) 20.3 mAs (d) 23.0 mAs (e) 25.0 mAs

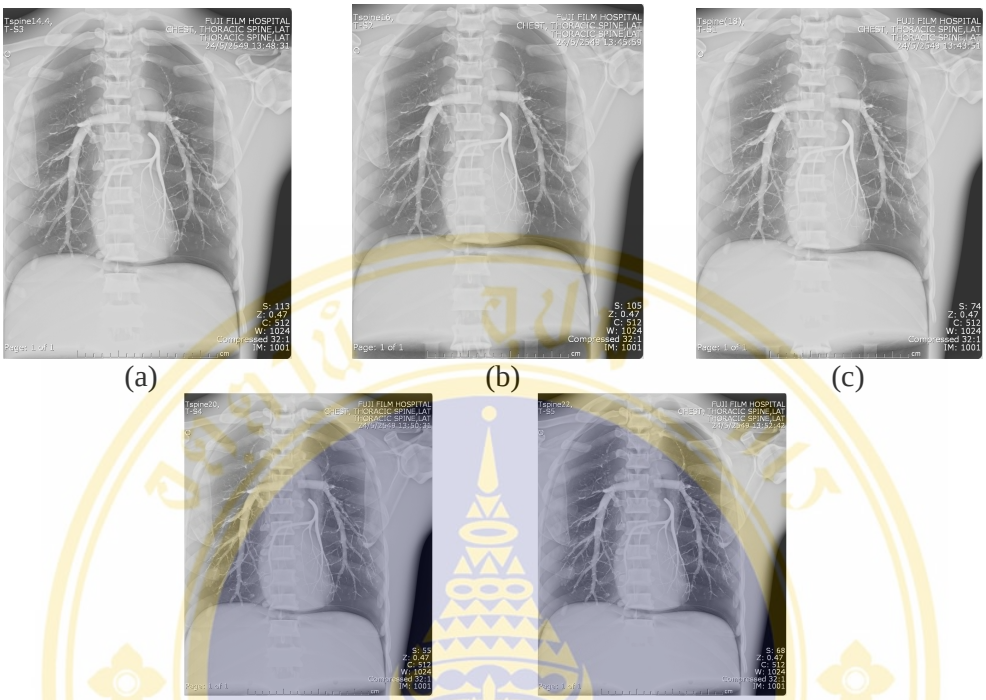

(a) (b) (c)

(d) (e)

Figure 26 Picture of Thoracic spine AP (a) 14.4 mAs (b) 16.0 mAs (c) 18.0 mAs (d) 20.0 mAs (e) 22.0 mAs

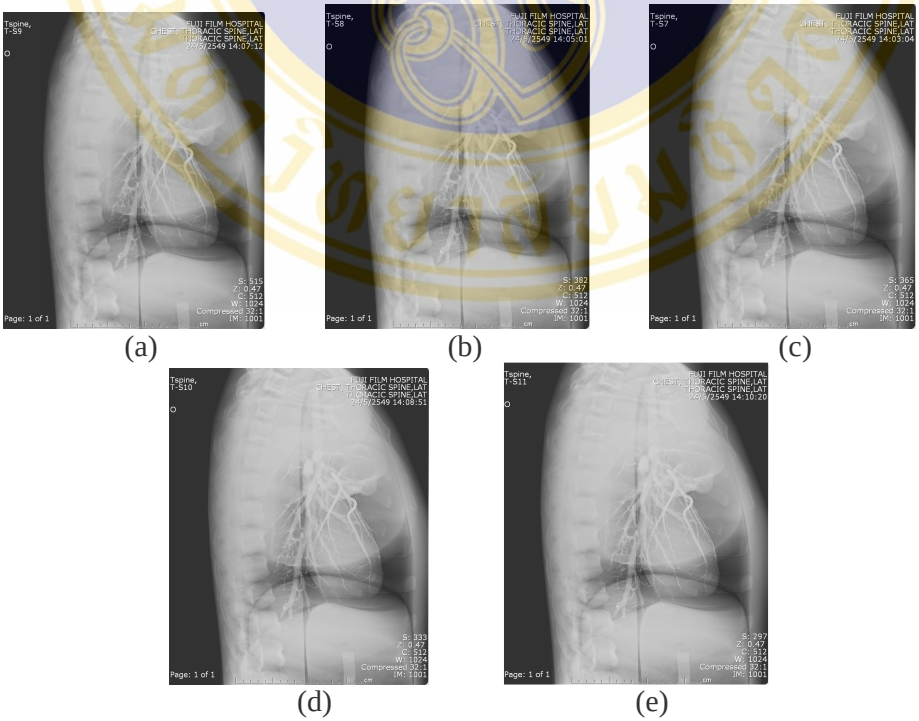

(a) (b) (c)

(d) (e)

Figure 27 Picture of Thoracic spine lateral (a) 21.4 mAs (b) 24.0 mAs (c) 27.2 mAs (d) 30.4 mAs (e) 32.0 mAs

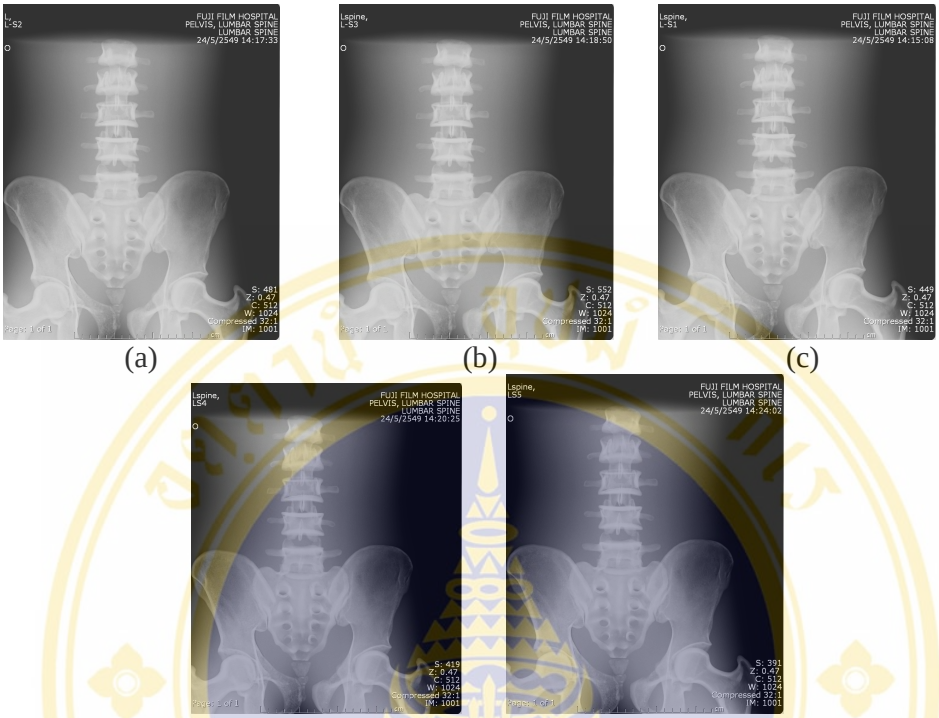

(a) (b) (c)

(d) (e)

Figure 28 Picture of Lumbar spine AP (a) 18.8 mAs (b) 21.2 mAs (c) 22.8 mAs (d) 25.2 mAs (e) 26.8 mAs

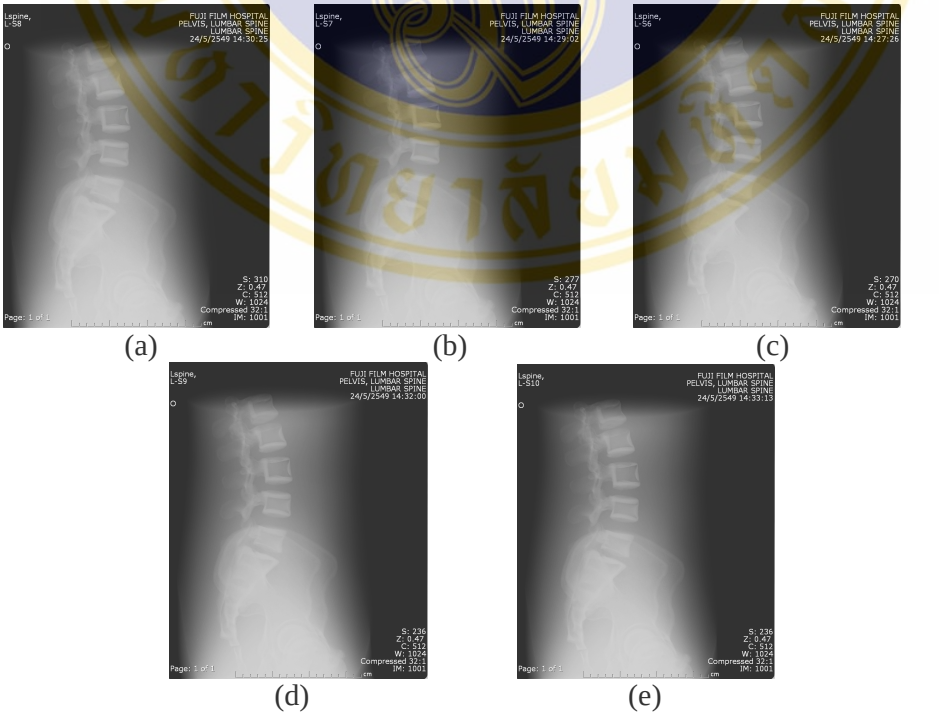

(a) (b) (c)

(d) (e)

Figure 29 Picture of Lumbar spine lateral (a) 27.8 mAs (b) 32.0 mAs (c) 34.6 mAs (d) 37.8 mAs (e) 40.6 mAs

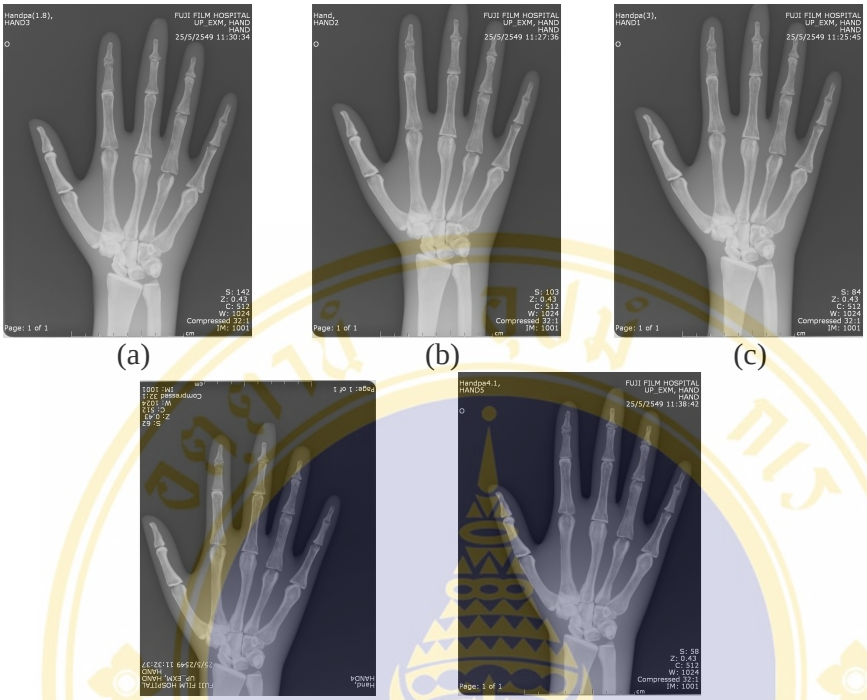

(a) (b) (c)

(d) (e)

Figure 30 Picture of Hand PA (a) 1.8 mAs (b) 2.4 mAs (c) 3.0 mAs (d) 3.8 mAs (e) 4.1 mAs

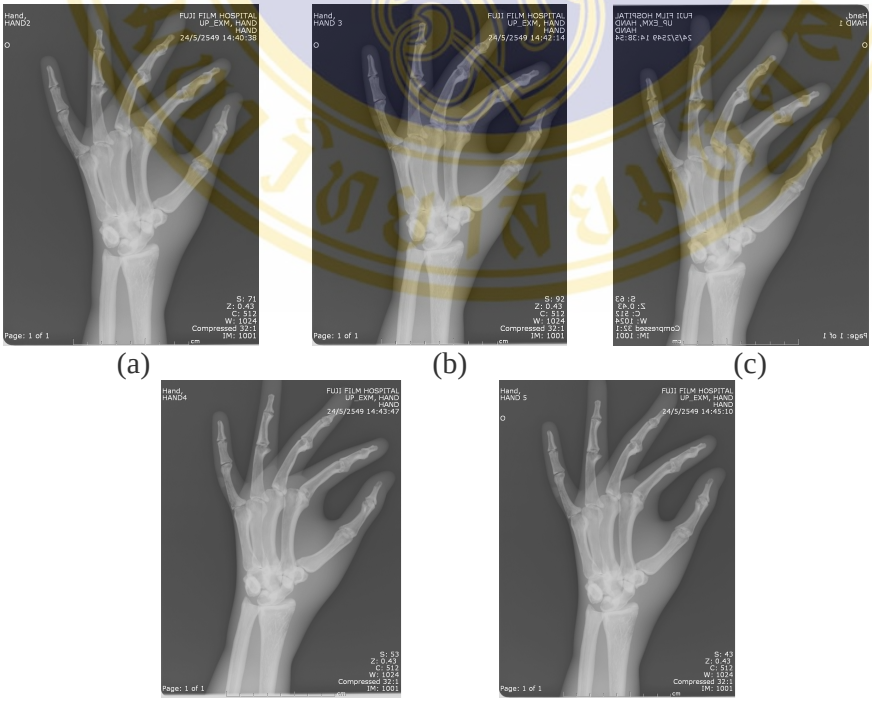

(a) (b) (c)

(d) (e)

Figure 31 Picture of Hand oblique (a) 3.0 mAs (b) 3.8 mAs (c) 4.1 mAs (d) 4.8 mAs (e) 6.0 mAs

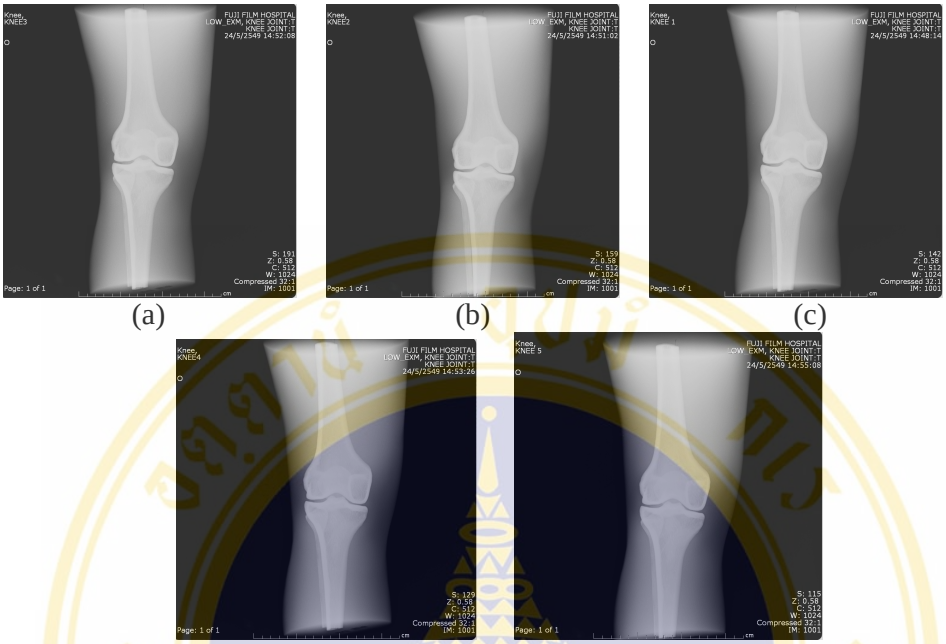

(a) (b) (c)

(d) (e)

Figure 32 Picture of Knee joint AP (a) 3.5 mAs (b) 4.1 mAs (c) 4.5 mAs (d) 4.9 mAs (e) 5.4 mAs

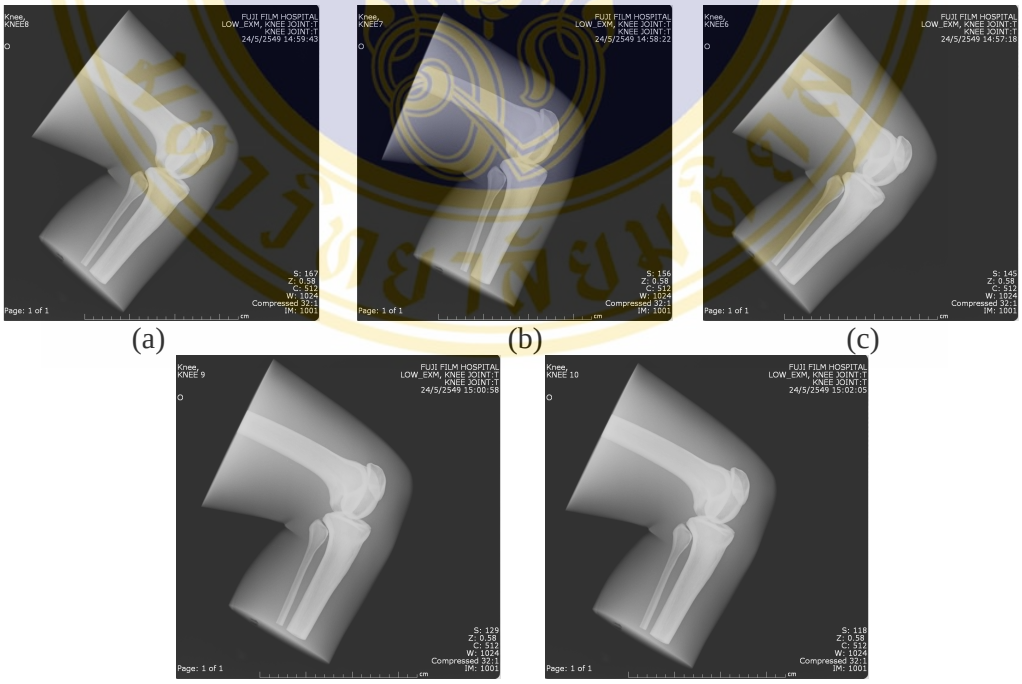

(a) (b) (c)

(d) (e)

Figure 33 Picture of Knee joint lateral (a) 3.5 mAs (b) 3.8 mAs (c) 4.1 mAs (d) 4.5 mAs (e) 4.9 mAs

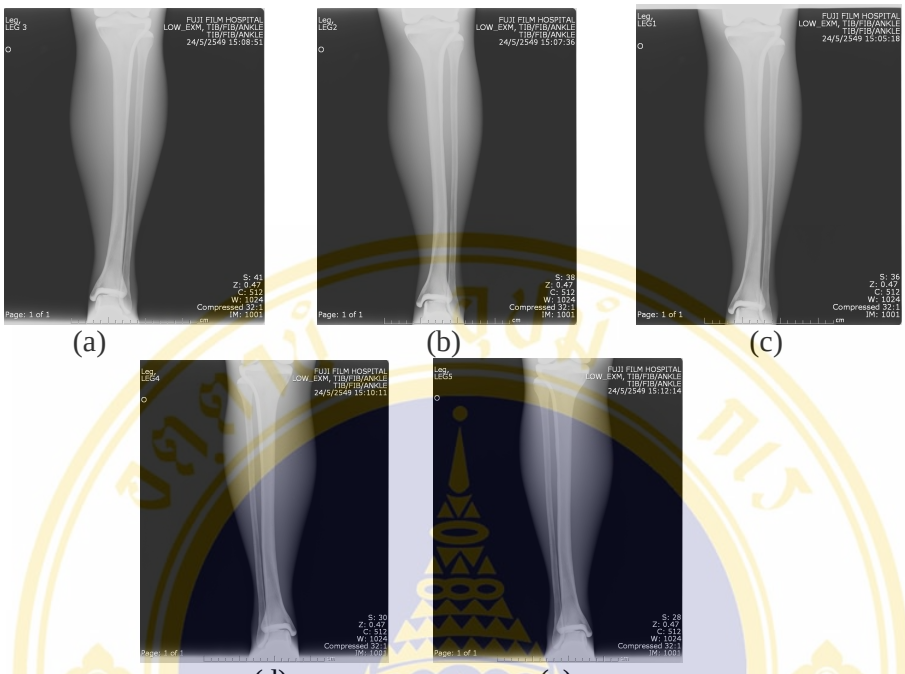

(a) (b) (c)

(d) (e)

Figure 34 Picture of Lower leg AP (a) 10.9 mAs (b) 12.0 mAs (c) 13.10 mAs (d) 15.0 mAs (e) 17.0 mAs

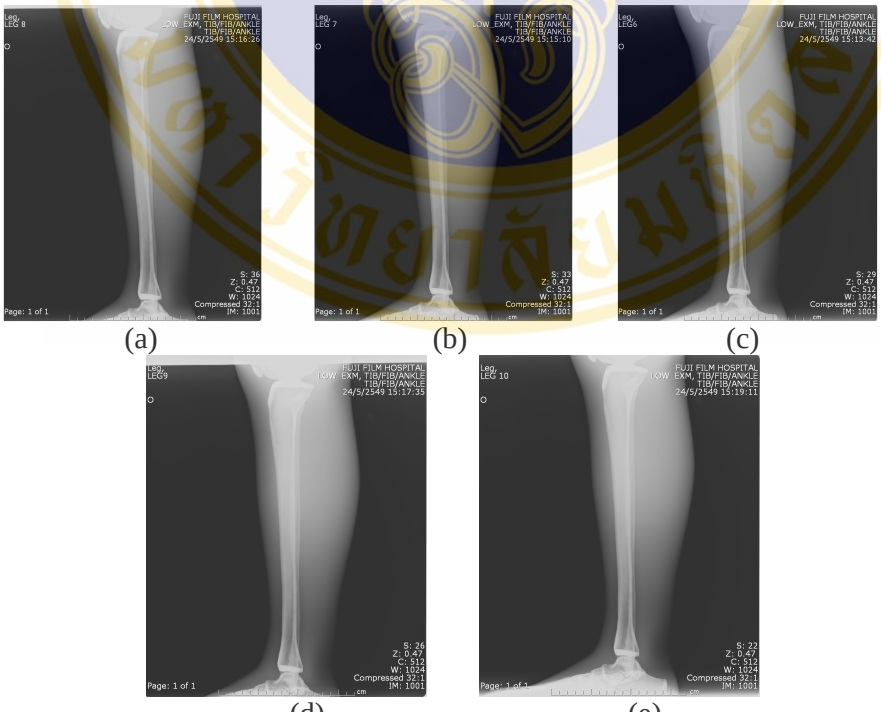

(a) (b) (c)

(d) (e)

Figure 35 Picture of Lower leg lateral (a) 10.9 mAs (b) 12.0 mAs (c) 13.10 mAs (d) 15.0 mAs (e) 17.0 mAs

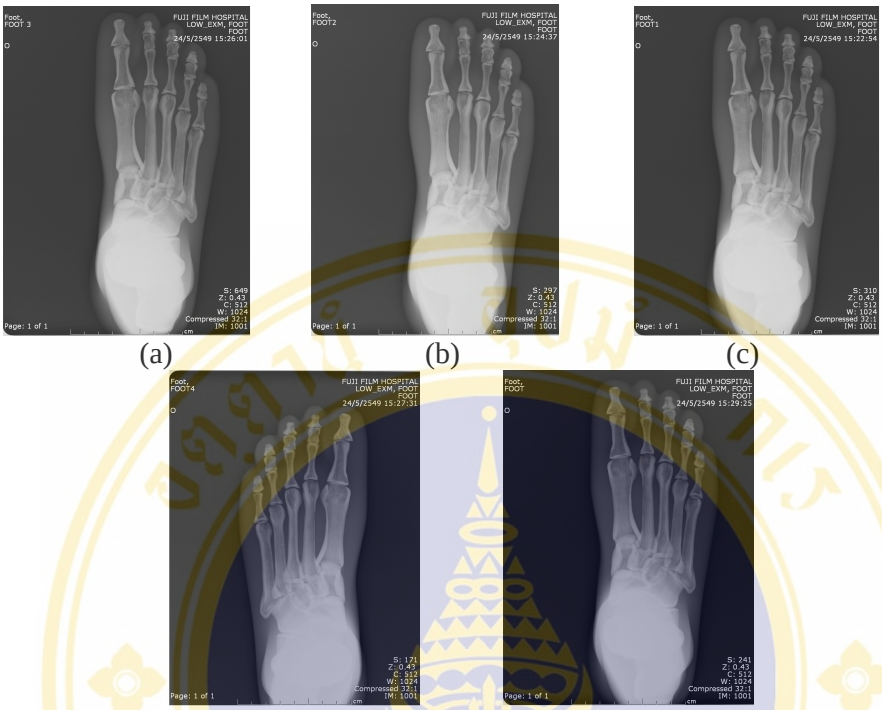

(a) (b) (c)

(d) (e)

Figure 36 Picture of Foot PA (a) 1.8 mAs (b) 2.4 mAs (c) 3.0 mAs (d) 3.8 mAs (e) 4.1 mAs

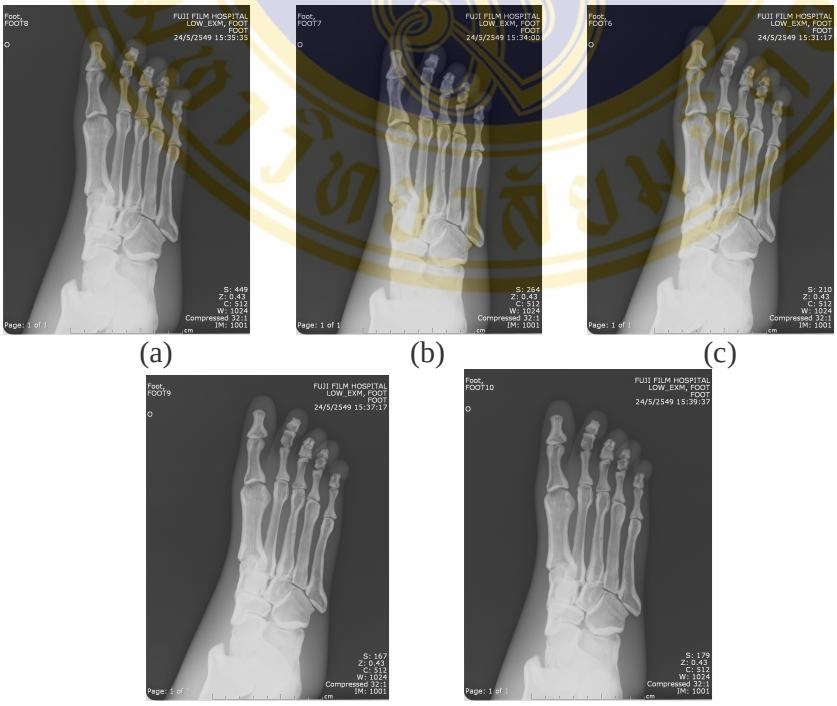

(a) (b) (c)

(d) (e)

Figure 37 Picture of Foot oblique (a) 1.8 mAs (b) 2.4 mAs (c) 3.0 mAs (d) 3.8 mAs (e) 4.1 mAs

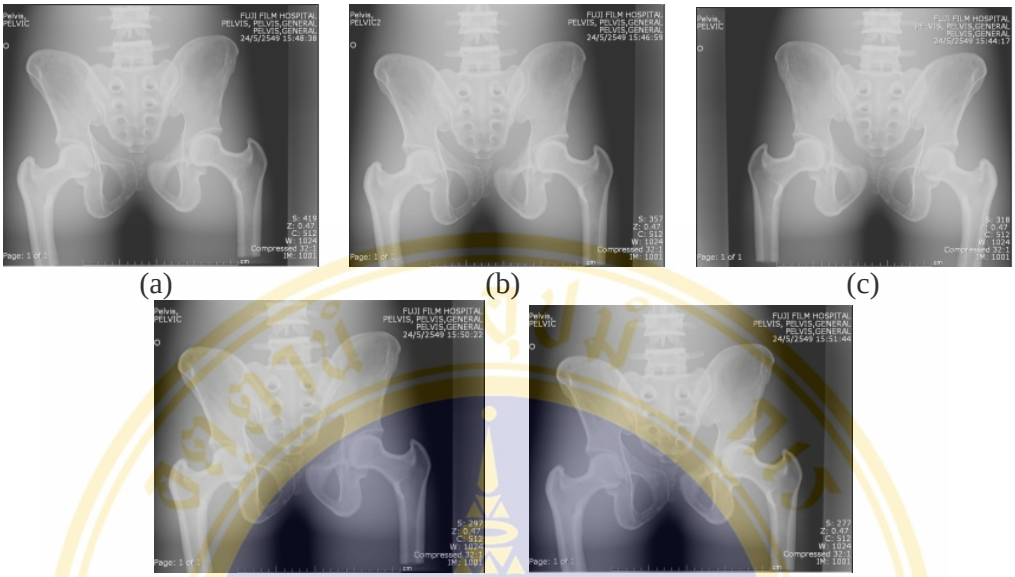

(a) (b) (c)

(d) (e)

Figure 38 Picture of Pelvic AP (a) 20.0 mAs (b) 22.8 mAs (c) 24.8 mAs (d) 27.2 mAs (e) 30.0 mAs

In the line with the results, the checklists prepared for further clinical quality evaluation experienced some modification following those checkpoints as preferred by the radiologist. By this means that, the tool or the checklist excluded clinical statements associated with unwanted features in phantom images that were not agree with the normal clinical requirements. Thus, the only important clinical aspects were critically restated. Therefore, as described in the table 4, several justified items about improperly clinical quality criteria were also clarified, base on the radiologist's suggestion.

It has been recognize that, there were 85 radiographs in selected technique procedures that allowed undertaking radiologist evaluation. The radiographs were judged by the radiologist that the radiologist choosing one of the marks avaliable in the checklist to which evaluated statement "yes" or "no" with the CQCI (Clinical Quality Criteria Index) in each position. The entire data about CQCI values can be seen in table 9.

Table 9 CQCI data of 17 position produced by means of the selected technique procedures

ROI / VIEW	CQCI(1)	CQCI(2)	CQCI(3)	CQCI(4)	CQCI(5)
1. skull : AP axial	1	1	1	1	1
2. skull : lateral	1	1	1	1	1
3. chest PA	0.2	0.2	0.4	0.6	0.6
4. chest lateral	1	1	1	1	1
5. thoracic spine : AP	0.6	1	0.6	1	0.6
6. thoracic spine :Lateral	0.67	0.5	0.67	0.5	0.5
7. lumbar spine : AP	1	1	1	1	1
8. lumbar spine : Lateral	1	1	1	1	1
9. hand : PA	1	1	1	1	1
10. hand : oblique	1	1	1	1	1
11. knee joint : AP	1	1	1	1	1
12. knee joint : Lateral (flex)	1	1	1	1	1
13. lower leg : AP	1	1	1	1	1
14. lower leg : lateral	1	1	1	1	1
15. foot : PA	1	1	1	1	1
16. foot : oblique	1	1	1	1	1
17. pelvic AP	1	1	1	1	1

Base on the summarized data in table 7, CQCI values for AP axial skull, lateral skull, chest lateral, AP lumbar spine, lateral lumbar spine, PA hand, oblique hand, AP knee joint, lateral (flex) knee joint, AP lower leg, lateral lower leg, PA foot, oblique foot and AP pelvic were equal to 1.00 in every values of adjusted exposures. This means no matter the value of exposure was increased or decreased; the clinical criteria can still be satisfied in the acquired radiographs.

For radiograph of PA chest, the value were increased when incresed the exposure. When the exposure was increased, the clinical quality of the image was found better. In contrast, for AP T-spine and lateral T-spine, the values of CQCI were not increased when the exposure was increased. This maybe due to the limitation of CR system since the auto-mode was employed instead of the fixed mode.

Overall results for clinical image quality show that increasing or decreasing radiation exposure to IP do not affect clinical image score except in chest PA and T spine examinations. This implies that based on clinical judgement using human mimicking phantom, radiation exposure can possibly reduced by 20% from standard screen-film techniques.

However, our clinical quality criteria were based on real human anatomy, which can be slightly different from the phantom model. Some critical organs or respiratory effects cannot be detected. Some of the image criteria have been reduced or adjusted to fit the phantom model. This implies that our results can be applied to use in clinical setting as a starting guideline. Radiograhic quality evaluation from real patients should be carried out using information provided by the phantom model for optimal quality of clinical images.

CHAPTER 6
CONCLUSION

The objective of this study was to evaluate physical and clinical performance of a Fuji XG-1 computed radiography system with aims to assess physical and clinical image quality. Physical phantom models were employed to evaluate image quality in terms of high contrast resolution, low contrast detectability and Modulation Transfer Function (MTF). In clinical performance evaluation, total of 85 radiographs obtained from anthropomorphic phantom were assessed for image quality in terms of clinical quality composite index (CQCI) by a qualified radiologist Blinded to the experiment. The measurements of Entrance Skin Air Kerma (ESAK) were also independently performed to assess the absorbed dose values from each radiographic examination. The results from this study showed that;

6.1 High contrast resolution

Selection of image plate size and direction of scan image plate has an impact on the clinical image quality. The results showed that decreasing image plate size improves spatial resolution. The changing in direction scan was found insignificant in improving the resolution. In digital imaging, limited resolution is primarily based on the pixel size. In clinical practice, there are other factors such as focal spot selection, patient inherent factors and technical settings can affect resolution. Evaluating limiting resolution qualitatively by using resolution test patterns ensure that radiologists can interpret the image with confidence for small object detected or fine details of the structures.

6.2 Low contrast detetability

The wide dynamic range of a CR system allows a hight tolerance for variations in exposure techniques. Typically, as we reduce the radiation exposure, the resultant image has more noise. Therefore, optimal exposure techniques are needed to ensure the best image quality at the lowest possible patient exposure. This work employed

two different phantoms (UAB phantom and custom made Low contrast detectability phantom) as tools to evaluate low contrast detectability. We concluded from the results that when radiation exposure increases, the contrast detail detectability can be improved. Optimal exit exposure to the image plate was found at 2 mR for regular size patient

6.3 Modulation Transfer Function (MTF)

Measurements of systems MTF at 20% were employed to delineate spatial frequency responses of the FUJI XG-1 CR system using different sizes of image plates in both scan lines. MTF. Results correlate well with results obtained from spatial resolution study. Small imaging plate size provides better hi frequency response. In contrast, MTF measurements can show differences of spatial resolution between the laser scan directions. Regarding effects of scan direction, MTF from the sub-scan direction were superior than the scan direction in big size IP (35 x 43 cm^2 and 35 x 35 cm^2). In small IP (18 x 24 cm^2), different scan directions do not provides significant differences.

6.4 Radiation Exposure (ESAK)

Results showed that ESAK values obtained from all radiographic examination were under IAEA guidance levels. Image quality obtained from 20% variation of ESAK was also found insignificantly difference.

6.5 Clinical performance characterization

No significant correlation was found between the patient dose and clinical quality composite index (CQCI). Overall results for clinical image quality show that increasing or decreasing radiation exposure to IP do not affect clinical image score except in chest PA and T spine examinations. This implies that based on clinical judgment using human mimicking phantom, radiation exposure can possibly reduced by 20% from standard screen-film techniques.

REFERENCES

1. Ballinger PW. Merill's Atlas of Radiographic Position and Radiologic Procedures. Vol.1, 3.10th ed. USA:Mosby; 2003.
2. Sonoda M, Takano M, Miyahara J, Kato H. Computed radiography utilizing scanning laser stimulated luminescence. Radiology 1983; 148:833-8.
3. Barnes GT. Digital x-ray image capture with image intensifier and storage phosphor plates:imaging principles, performance and limitations. Digital imaging (AAPM Monograph):1993; 22:23-48.
4. Fujita H, Ueda K, Morishita J, Fujikawa T, Ohtsuk A, Sai T. Basic imaging properties of a computed radiograpic system with photostimulable phosphors. Med Phys. 1989; 16:52-9.
5. Bushberg JT, Seibert JA, Leidholdt EM, Boone JM. The essential physics of Medical imaging. 2nd ed. Philadelphia:Lippincott&Wilkin;2002.
6. Ruggiero C. A teleradiology Primer. Teleradiology.1998; 4:25-35.
7. Gregg EG. Visual response of the interpreter. Quantitative Organ Visualization in Nuclear Medicine. Miami:University of Miami Press; 1971.
8. Barlow HG. The efficiency of detecting changes in density and random dot patterns. Vision Res 1987:637.
9. Rose A. The sensitivity if the human eye on an absolute scale. J Opt Soc Am 1948:196-208.
10. Greene RE, Oestmann JW, Rubens JR. High frequency edge enhancement in the detection of fine pulmonary lines:Parity between storage phosphor digital images and conventional chest radiography. Invest Radiol 1989; 643-646.
11. Greene RE, Oestmann JW. Computed Digital radiography in Clinical Practice. New York. Thieme Medical Publishers; 1992.
12. Lancaster JL. Radiological sciences graduate program. Chapter 4. San Antonio:Research Imaging Center; 1990.

13. Lancaster JL. Radiological sciences graduate program. Chapter 8. San Antonio:Research Imaging Center; 1990.
14. Interagency Working Group on Medical Radiation. Radiation protection guidance for diagnostic x-ray. Washington:1976.
15. Samei E, Seibert JA, Willis CE, Flynn MJ, Mah E, Junck KL, Performance evaluation of computed radiography system. Med Phys 2001; 28:361-7.
16. Anthony JW, Gary TB, Wu X, Assessing fluoroscopic contrast resolution:A practical and quantitative test tool. Med Phys 1991; 18:894-99.
17. Lu ZF, Nickoloff EL, So JC, Dutta AK, Comparision of computed radiography and film/screen combination using a contrast-detail phantom. Journal of Applied Medical Physics 2002; 4:91-8.
18. Koenig A, Gliere A. Radiographs simulation using system MTF. France.
19. Sanfridsson J, Holje G, Svahn G, Ryd L, Jonsson K. Radiation dose and image information in computed radiography-a phantom study of angle measurements in the weight-bearing knee. ActaRadiol 2000; 41:310-16.
20. BICRON. Anthropomorphic phantoms for teaching/training in diagnostic radiology. Bicron Technologies Vertriebs-GmbH:Germany.
21. AAPM Report No.31 Basic Quality Control in Radiology. AAPM; New York: 1977.
22. Pongnapang N. Computed radiography image reader performance. Bangkok;2006.
23. Samei E. Acceptance testing of computed radiography (CR) system;1997.
24. International Atomic Energy Agency. International basic safety standards for protection against ionizing radiation and for the safety of radiation sources. Vienna: Austria; 1996.
25. Quantum Medical Imaging. Quest HF seriesTM X-ray Generators. New York; 2004.
26. A web module produced by committee 3 of the International Commission on Radiological Protection (ICRP). Diagnostic reference levels in medical imaging; 2001.
27. Moeller TB. Normal findings in Radiography. New York:Thieme Stuttgart 2000.
28. Ballinger PW, Merill's Atlas of radiographic positions and radiologic procedures. 6th ed. Saint Louis: Mosby; 1995.

29. AlmenA, Tingberg A, Mattsson S, Besjakov J, Kheddache S, Lanhede B, et al. The influence of different technique factors on image quality of lumbar spine radiographs as evaluated by established CEC image criteria. Br J Radiol 2000; 73:1192-9.

APPENDIX

APPENDIX

Quality control program of the x-ray machine and facilities

The sections below described and discussed about the results of quality control program.

1.1a. Visual check of the facility

Visual checking for the readiness of the x-ray facilities was performed daily during the period of the experiments. These may include accuracy of focal-to-image distance indicator, accuracy and function angulation indicator, function and effectiveness of table and all other locks, condition of high voltage and other cables, ease of overhead crane movement and proper function of bucky-cassette lock. The operational system of the x-ray machine and processor were inspected at glance and confirm their general conditions before used in the experiments.

1.2a. Quality control tests of the x-ray generator

A typical general purpose x-ray unit from the Quantum medical imaging Quest HF series equipped with AEC devices underwent testing procedure to ensure its current performance reliability before used for the experimental radiography in this study. Owing to technical data, the x-ray generator is operated with 1 phases, and high frequency. Tube rating for maximum kVp is 150, while dual focal spot dimension (the large size 1.2 mm and the small size 0.6 mm) is selectable. Typical filter are attached to the x-ray tube that consists of an inherent 0.9 mm of Aluminum filters applied for 75 kV. The priority off test was mainly emphasized on the evaluation of the five technical parameters of the x-ray generator: the focal spot measurement, consistency of tube current, accuracy and precision of tube voltage, accuracy and precision of the exposure time and the beam quality (HVL). The following informs the results of measurements.

Table 1a. Consistency of the tube current

QC Tool: Full function meter RMI 242

Objective: to evaluate the consistency of the tube current (mAs) from varying mA station

Technique: Technique1; kVp 80; mA 100; mAs 20

Technique2; kVp 80; mA 200; mAs 20

FFD 100 cm

Acceptance limit: ± 10%

Number of exposure	Measured in mR	
	Technique 1	Technique 2
1	313	308
2	313	308
3	313	308
4	312	308
5	313	308
6	313	308
7	312	309
8	313	308
9	312	308
10	312	308
Mean	312.6	308.1
MR/mAs	15.63	15.41
Acceptance	YES	

Table 2a. The tube voltage accuracy and precision

QC Tool: Full function meter RMI 242

Objective: 1. kVp accuracy; to determine that the machine is producing the kVp selected on the control panel

2. kVp precision; to determins that the kVp is consistent from exposure to exposure

Acceptance limit: Accuracy $\leq \pm 5$ % ; Precision ≤ 5 %

Technique: mAs at 10; kVp vary; FFD 100 cm.

Number of exposure	Selected kVp					
	50	60	70	80	90	100
1	50.1	60.2	70.3	81.1	91.4	101.9
2	49.8	60.1	70.4	81.8	91.9	102.6
3	51.4	60.4	70.7	81.2	90.4	102.7
4	50.2	60	70.4	81.4	91.5	102.3
5	50.5	60.2	70.7	81.4	90.9	102.3
Mean	50.4	60.18	70.5	81.38	91.22	102.36
Accuracy(%)	0.800	0.300	0.710	1.725	1.356	2.36
Precision(%)	1.220	0.250	0.270	0.330	0.640	0.310
Acceptance	YES	YES	YES	YES	YES	YES

Table 3a. The exposure time accuracy and precision

QC Tool: Full function meter RMI231A

Objective: to evaluate accuracy and precission of the exposure time

Acceptance limits: Accuracy $\leq \pm 5$ % ; Precision ≤ 3 %

Technique1: kVp 60;FFD 100 cm: mA 100;ms 50

Technique2: kVp 60;FFD 100 cm: mA 200;ms 50

Technique3: kVp 60;FFD 100 cm: mA 100;ms 100

Technique4: kVp 60;FFD 100 cm: mA 200;ms 100

Table 3a. The exposure time accuracy and precision (Continued)

Number of exposure	Technique 1	Technique 2	Technique 3	Technique 4
1	49.0	49.1	99.5	99.3
2	49.4	49.1	99.4	99.2
3	49.4	49.1	99.4	99.2
4	49.4	49.1	99.4	99.1
5	49.4	49.1	99.4	99.3
Mean	49.32	49.1	99.42	99.22
Accuracy	1.36	1.80	0.58	0.78
Precisions	0.36	0.00	0.04	0.084
Acceptance	YES	YES	YES	YES

Table 4a. Beam quality assessment

QC Tool: Full function meter RMI 242, Al HVL attenuator set M115A

Objective: to determine the half-value layer (HVL) of the x-ray beam

Technique: kV 80; mA 200; mAs 50

Thickness of aluminium	Reading at meter (mR)				
(mm)	1	2	3	4	5
open field	794	794	794	794	794
1.0 mmAl	636	636	636	635	636
1.5 mmAl	575	575	575	575	575
2.0 mmAl	523	523	524	523	524
2.5 mmAl	477	479	478	479	478
3.0 mmAl	445	445	445	445	445
3.5 mmAl	410	408	409	408	408
4.0 mmAl	379	378	379	378	378

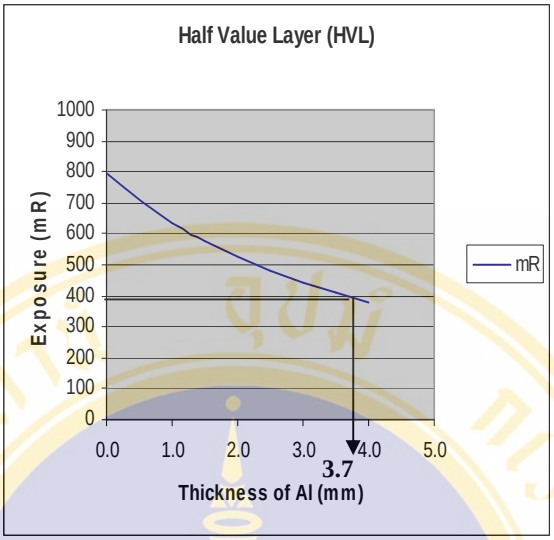

Figure 1a. Half Value Layer

1.3a. Radiographic tests

The radiographic tests mentioned here were focused on the tests for the collimator and beam alignment.The following two tables about the results of the collimator and beam alignment tests.

Table 5a. Collimator test

QC Tool : Collimator and beam alignment test tools

Objective : to assure that the light field and the x-ray field are congruent

Acceptance limit : $\leq$ 2 % of FFD ($\leq$ 1.8 cm)

Technique: selected field size at x = 18.00 cm, y = 13.00 cm

kV 80; mA 200; mAs 5

Long axis			Short axis		
X1	X2	% FFD(X1+X2)	Y1	Y2	%FFD (Y1+Y2)
0.5	0.2	0.7	0.4	0.4	0.8
Acceptance		YES	Acceptance		YES

Table 6a. Beam alignment test

QC Tool : Collimator and beam alignment test tools

Objective : to assure that the central point of the x-ray beam is aligned with the focal spot position

Acceptance limit : $\leq 3°$

Technique: selected field size at x = 18.00 cm, y = 13.00 cm
kV 80; mA 200; mAs 5

Ball image in 1st circle (1.5)	Ball image in 2st circle (3)	Outside of the cycle (>3)	Acceptance
YES	-	-	YES

The overhead tube crane, the table and some supporting facilities such as the table, control booth etc., were in good condition.

For the QC tests of x-ray generator, The consistency of the tube current, the results showed that the mR/mAs was much lesser than that from the accptance limit (Acceptance limit $\pm$ 10 %) at 80 kVp for rooms using the same type of x-ray generators,tubes, and tables. This showed a very consistent level of the mAs production.

For the tube voltage (kVp) evaluation, the x-ray machine provided a high accuracy and precision in term of six different selected levels of kV stations ranged from 50 kVp to 100 kVp. The percentage of accuracy varied about 0.3-1.7 % while the precision ranged approximately within 0.25-1.22 %. These percentages have accepted with the suggested levels that for the accuracy $\leq \pm 5\%$ and the precision $\leq 5\%$.

The exposure time accuracy and precision with two exposure time of four technique. The accuracy ranged about 0.58-1.8 % while the precision ranged varied about 0-0.36 %. These percentages have complied with the suggested levels that for the accuracy $\leq \pm 5$ % and the precision ≤ 3 %.

The half value layer (HVL) measurement was to figure out the capability of the x-ray beam in penetrating slabs of Aluminum thickness by which the hardness of the

x-ray beam. A 50 % of the exposure transmission was about 397 mR. Thus, the approximate HVL value reached at a value 3.7 mm of Aluminum at the tube potential 80 kV. Recommendation that provided by the food and Drug Administration (FDA) quoted in the NCRP report number 99 stated the HVL value at 80 kV should be at list 2.3 mm of Aluminum. As the measured HVL value was greater than that of the expected value, the beam quality was appropriate or safe enough in term of dose and image quality effects

For the collimator test, the percentages of the measured X-axes and Y-axes with respect to the Focus-Film Distance were found at the X = 0.7 % of the FFD and the Y = 0.8 % of the FFD. These results met the requirements of the NCRP recommendation. The test about alignment between the tube focus and the center of the x-ray field provided a vary convenience result where the image ball appeared in the first inner circle (or $\leq 3°$), the result definitely complied with the suggested limit. The collimator and beam alignments were satisfied.

The mR/mAs measurement

The measured mR/mAs at the table with bucky, table and the chest stand were estimated using the following the figure 1a

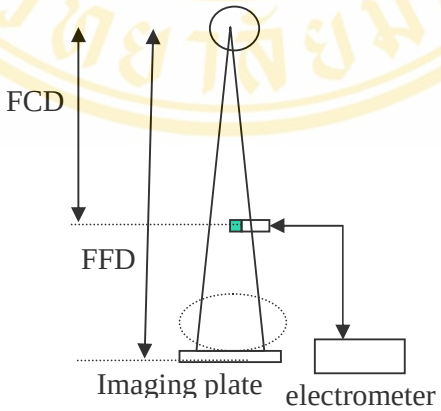

Figure 2a The geometry for the free-in-air measurements

Table 7a. Distance of mR/mAs measurement

Geometry	FCD	FFD
Table	70	100
Table, with bucky	63	100
Chest stand	150	180

FCD = Focal Chamber Distance
FFD = Focal Film Distance

Table 8a. The mR/mAs for the table with bucky

kV	mR/mAs at 3mAs measurement	mR/mAs at 5mAs measurement	mR/mAs at 10mAs measurement	mR/mAs
50	3.94	3.99	4.20	4.04
55	5.07	5.09	5.38	5.18
60	6.24	6.19	6.62	6.35
65	7.40	7.40	7.92	7.57
70	8.60	8.65	9.28	8.84
75	9.84	9.97	10.74	10.18
80	11.11	11.33	12.27	11.57
85	12.56	12.87	13.93	13.12
90	13.98	14.43	15.64	14.68
95	15.44	16.02	17.42	16.29

Table 9a. The mR/mAs for the table

kV	mR/mAs at 3mAs measurement	mR/mAs at 5mAs measurement	mR/mAs at 10mAs measurement	mR/mAs
45	2.31	2.35	2.47	2.38
50	3.12	3.17	3.34	3.21
55	4.02	4.03	4.28	4.11
60	4.93	4.92	5.26	5.04
65	5.86	5.88	6.31	6.02
70	6.78	6.86	7.38	7.01
75	7.73	7.9	8.55	8.06

Table 10a. The mR/mAs for the chest stand

kV	mR/mAs at 3mAs measurement	mR/mAs at 5mAs measurement	mR/mAs at 10mAs measurement	mR/mAs
95	2.66	2.72	2.91	2.76
100	2.94	3.03	3.22	3.06
105	3.24	3.33	3.54	3.37
110	3.55	3.61	3.87	3.68

BIOGRAPHY

NAME	Miss. Kumutinee Pairat
DATE OF BIRTH	16 February 1980
PLACE OF BIRTH	Rayong, Thailand
INSTITUTIONS ATTENDED	Mahidol University, 2002: Bachelor of Science (Radiological Technology) Mahidol University, 2006: Master of Science (Medical Physics)
POSITION&OFFICE	Radiosurgery Center 270 Ramathibodi Hospital, Bangkok, Thailand Position : Medical Physicist Tel. (02) 201-1742
HOME ADDRESS	4/35 Soi. Tewasuntorn Ladyoaw Jatujak Bangkok 10900